bioRxiv preprint doi: https://doi.org/10.1101/827519; this version posted November 2, 2019. The copyright holder for this preprint (which was not certified by peer review) is the author/funder. All rights reserved. No reuse allowed without permission.

Title

Interplay of bacterial membrane vesicle and host lipid physicochemical parameters during host-bacterial membrane vesicle interaction

Authors

Ashutosh Prince[1], Anuj Tiwari[1]†, Titas Mandal[1]†, Kuldeep Sharma[1], Nikhil Kanik[1], Deepak Kumar Sinha[2], Mohammed Saleem[3,4]*

Affiliations

[1]Department of Life Sciences, National Institute of Technology, Rourkela, India.

[2]Department of Biological Chemistry, Indian Association for the Cultivation of Sciences, Kolkata, India.

[3]School of Biological Sciences, National Institute of Science Education and Research, Bhubaneswar, India.

[4]Homi Bhabha National Institute, Mumbai, India.

† Equal contribution

* Corresponding Author, email: saleem@niser.ac.in

bioRxiv preprint doi: https://doi.org/10.1101/827519; this version posted November 2, 2019. The copyright holder for this preprint (which was not certified by peer review) is the author/funder. All rights reserved. No reuse allowed without permission.

Abstract

Bacterial membrane vesicles (MVs) facilitate long-distance delivery of virulence factors crucial for pathogenicity. The entry and trafficking mechanisms of virulence factors inside host cells is recently emerging, however, if bacterial MVs modulate the physicochemical properties of the host lipid membrane remains unknown. Here we quantitatively show that bacterial MV interaction increases the fluidity, dipole potential and elasticity of a biologically relevant multi-component host model membrane. The presence of lipids containing head-groups such as phosphatidylcholine, phosphatidylglycerol and phosphatidylinositol and a moderate acyl chain length of C16 helps the MV interaction. While significant binding of bacterial MVs to the raft-like lipid membranes with phase separated regions of the membrane was observed, however, the elevated levels of cholesterol tend to hinder the interaction of bacterial MVs. We further quantify the change in excess Gibbs free energy of mixing of bacterial MVs with host lipid membranes driving the modulation of host membrane parameters.

Keywords: Membranes; Vesicles; Bacterial Membrane Vesicles; Dipole Potential; GUV; Liposomes; Fluorescence Spectroscopy; Fluorescence Microscopy; Anisotropy; Compressibility Modulus.

bioRxiv preprint doi: https://doi.org/10.1101/827519; this version posted November 2, 2019. The copyright holder for this preprint (which was not certified by peer review) is the author/funder. All rights reserved. No reuse allowed without permission.

Introduction

The secretion of membrane vesicles (MVs) from the bacterial cells is recognized as a generalized phenomenon observed in many bacteria, particularly Gram negative bacteria [1, 2]. Bacterial MVs released by the Gram negative bacteria are known to facilitate contact-free inter-species communication, nutrient acquisition, enhanced survival against immune response and host-pathogen interaction[3]. Bacterial MVs were initially known to be only secreted by controlled blebbing of Gram negative bacteria and referred to as Outer membrane vesicles (OMVs), however, more evidence is emerging in support of existence of different types of Bacterial MVs, such as – Bacterial MVs, Outer-inner membrane vesicles (OIBMVs) and Explosive outer membrane vesicles (EOBMVs) all of which are involved in transport of virulence factors[4]. Typically, bacterial MVs are nano-sized spherical membrane compartments spanning 20-300 nm in diameter derived from the outer membrane lipid bilayer and the periplasm of the bacteria[3]. Biochemically, bacterial MVs are known to carry lipopolysaccharides (LPS), phospholipids, peptidoglycans, outer membrane proteins (OMPs), nucleic acids, signaling molecules and periplasmic, cytoplasmic and membrane-bound proteins[5]. The degree of bacterial MV secretion has also been correlated to the pathogenicity and virulence of bacteria[6]. Interestingly, in addition to delivering a selection of virulence factors and immunomodulatory molecules directly into host cells during infection, bacterial MVs are also known to act as decoy antigen and divert the host immune system away from the bacterial cell [7]. There is a considerable focus on the understanding of the virulence factors of the MV cargo and modes of bacterial MV entry inside host cells. Owing to a wide range of size of bacterial MVs, different pathways such as macropinocytosis, clathrin-dependent and caveolin or lipid raft mediated endocytosis have been implicated in the internalization processes of different Bacterial MVs [8]. Further, direct membrane fusion with host cell membranes, preferentially at lipid raft domains, has also been reported to be a potential mechanism of entry of bacterial MVs [9]. Similarly, fusion of bacterial MVs extracted from *L. pneumophila* with host model membranes suggested the faster time scales of fusion events (few seconds), which is also temperature-dependent [10].

The existence of considerable discrepancies in observations of the multiple entry routes of bacterial MVs inside host cells suggest existence of multitude of mechanisms that effect host machinery. A crucial aspect that remains unexplored is if/how MV fusion

bioRxiv preprint doi: https://doi.org/10.1101/827519; this version posted November 2, 2019. The copyright holder for this preprint (which was not certified by peer review) is the author/funder. All rights reserved. No reuse allowed without permission.

modulates the physicochemical parameters of host cell membranes (i.e., fluidity, dipole potential and elasticity)? Irrespective of the kind of bacterial MVs, mode of entry of bacterial MVs, insights on membrane interfacial interaction of bacterial MVs is crucial as the local lipid reorganization and remodeling of the host cell membrane is a prerequisite for MV entry. It is proposed that the MV fusion may result in changes in the properties of the host cell membrane[10], however, the host membrane lipid specificity of the MV interaction, and quantitative changes in host membrane fluidity, dipole potential and elasticity triggered by bacterial MVs is lacking.

This work reports for the first time, to best of our knowledge, MV mediated modulation of host lipid membrane fluidity, dipole potential and elasticity. Further, we also report the specific role of host membrane lipid head-group charge, acyl chain and phase separated boundaries on the interfacial interaction of bacterial MVs. Using *in vitro* reconstitution, fluorescence microscopy, potentiometric dye-based fluorescence anisotropy and dipole potential measurements and Langmuir monolayers, we show that MV interaction increases the fluidity, dipole potential and elasticity of the host model membranes. Such modulation is particularly facilitated by the presence of lipids such as DOPC, DOPG and Liver PI as well as the acyl chain preference for C16. We also find that entry of bacterial MVs has preference for liquid disordered regions of the lipid membrane. Further, elevated levels of cholesterol in raft-like lipid membranes with phase separated regions tend to hinder the interaction of bacterial MV. The surface pressure-area isotherms further quantitatively revealed the change in Gibbs excess free energy of mixing of MV components with varying host membrane lipid membranes and the subsequent modulation of elasticity in each case.

bioRxiv preprint doi: https://doi.org/10.1101/827519; this version posted November 2, 2019. The copyright holder for this preprint (which was not certified by peer review) is the author/funder. All rights reserved. No reuse allowed without permission.

Results

Bacterial membrane vesicle (MV) fusion increases the fluidity and dipole potential of host model membrane

Bacterial membrane vesicles have been reported to enter host cells via multiple routes such as endocytosis, micropinocytosis and fusion in different cell types [11]. Here, we sought to elucidate the lipid specificity and modulation of host membrane properties by bacterial MV interaction which remains central to all routes of entry yet remains unexplored. We used *E. coli* as a model Gram negative bacterium for the isolation of bacterial MVs and set out to systematically investigate the interaction of bacterial MVs with host membranes (Figure 1A). Bacterial MVs were isolated by means of chemically induced vesiculation (as described in methods). The characterization of the size heterogeneity of bacterial MVs was carried out by fluorescence-based pixel size estimate, dynamic light scattering and electron microscopy. To this end, bacterial MVs were labeled with 1% (v/v) 3,3′-dioctadecyloxacarbocyanine perchlorate (DiO), a fluorescent lipophilic dye, and visualized by confocal microscopy after filtering out the free unbound dye. The observed size of bacterial MVs was found to be approximately of ~200 nm in diameter, extracted through estimated pixel spread of the observed fluorescence signal in the confocal images using image J (Figure 1C). The estimated size of bacterial MVs was further corroborated by dynamic light scattering showing an intensity maximum of ~200 nm (Figure 1B), further, confirmed by electron microscopy (Figure 1D). We additionally confirmed bacterial MVs presence by labeling with Nile Red, another lipophilic membrane dye, that fluoresces only under lipid-rich environment (Figure 1E, and Figure S1)[12]. We then confirmed the internalization of bacterial MVs by human macrophages, as also reported earlier [10]. The labelled bacterial MVs (devoid of any free unbound dye) were incubated with the macrophage cells in cell media for a period of about 2.5 hours to monitor the changes in the bacterial MV fluorescence arising in the cell media. Measurement of fluorescence intensity of a fixed volume of isolated cell media every 30th minute revealed a gradual yet linear decrease in the fluorescence arising from the residual labelled MV (Figure 1F). This methodology also provides an indirect measure of the kinetics of the bacterial MV fusion with the macrophage cells. Fluorescence bleaching can be ruled out as no significant change in fluorescence of the cell media containing MV was observed in the absence of macrophage cells (Figure 1F).

bioRxiv preprint doi: https://doi.org/10.1101/827519; this version posted November 2, 2019. The copyright holder for this preprint (which was not certified by peer review) is the author/funder. All rights reserved. No reuse allowed without permission.

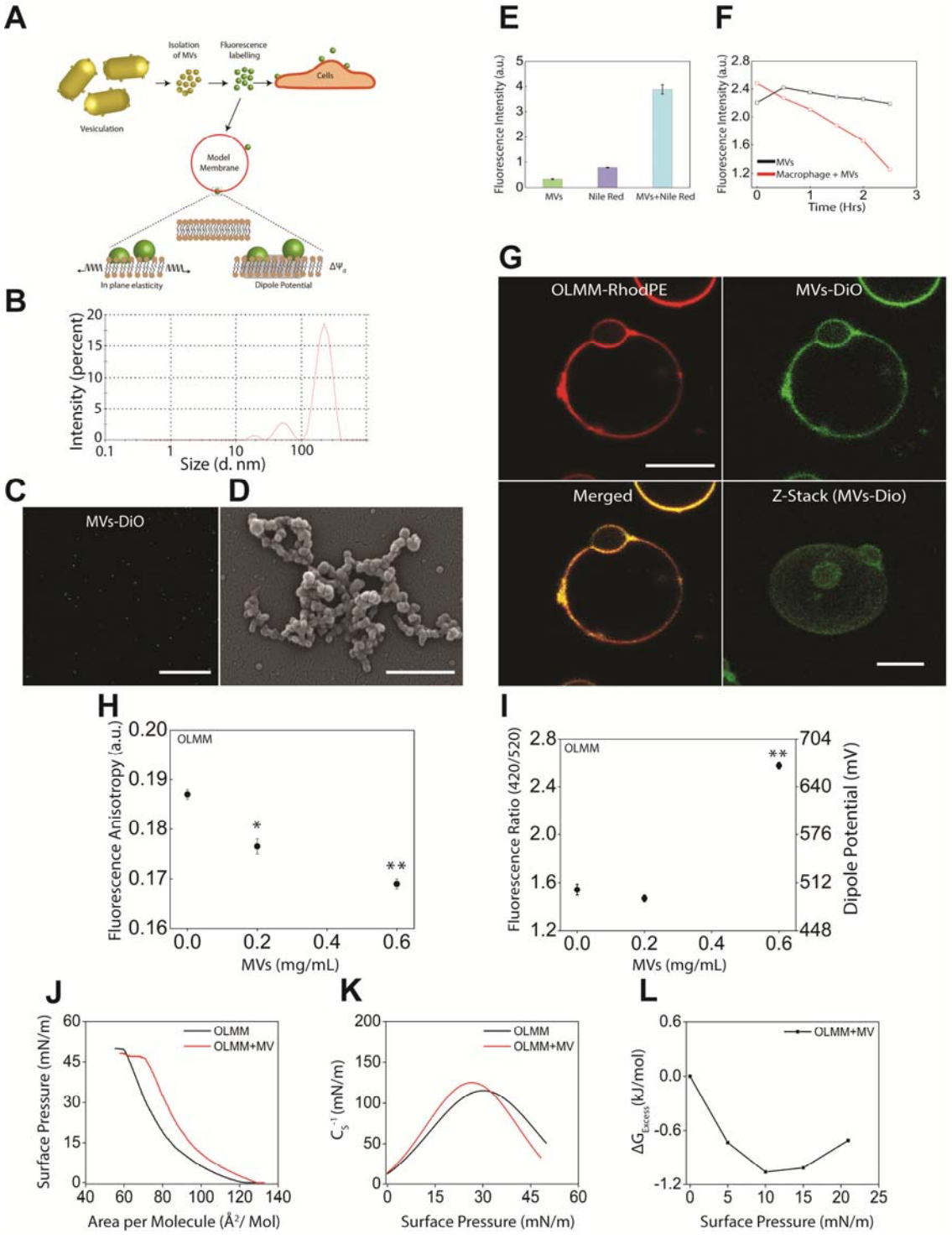

Figure 1. Characterization of bacterial Membrane Vesicles (MVs) isolated from *Escherichia coli*, internalization of bacterial MVs in macrophages and their effect on membrane binding, fluidity, dipole potential and Surface Pressure (π) - Mean

bioRxiv preprint doi: https://doi.org/10.1101/827519; this version posted November 2, 2019. The copyright holder for this preprint (which was not certified by peer review) is the author/funder. All rights reserved. No reuse allowed without permission.

molecular area (A) isotherm, compressibility modulus and excess Gibb's free energy change of reconstituted outer leaflet model membrane of host cell. **(A)** Schematic summarizing the methodology used to isolate, fluorescently label and study the MV-host membrane interaction. **(B)** Size distribution of bacterial MVs measured by dynamic light scattering. **(C)** Confocal image of DiO labelled MV suspension (Scale bar - 10 µm). **(D)** Electron micrograph of Bacterial MVs Isolated and filtered from *E. coli* (scale bar - 1µm). **(E)** Comparative fluorescence intensities of unlabelled Bacterial MVs, Nile red and Bacterial MVs incubated with Nile red which increased in presence of Bacterial MVs. **(F)** Fluorescence intensity of Nile red labelled Bacterial MVs (Black line) and Nile red labelled Bacterial MVs incubated with macrophages to confirm uptake of Bacterial MVs by the macrophage for 2.5 hours (Red line). **(G)** Confocal images of reconstituted GUVs of outer leaflet model membrane (OLMM-RhodPE) composed of DOPC 35 mole %, DOPE 5.6 mole %, Brain SM 20 mole %, Cholesterol 30 mole % doped with 1 % Rhodamine PE (*red channel*) mimicking outer leaflet of eukaryotic cell membrane. Bacterial MVs labelled with DiO binding to the GUVs (green channel) distributed homogenously over the equatorial plane of GUVs along with merged image of both red and green channels showing a co-localisation. 3D-stack of the OLMM GUVs (Green channel). Fluorescence imaging were done thrice independently and at least 30-35 GUVs were observed under microscope (scale bar - 10µm). **(H)** Fluorescence anisotropy of OLMM decreases with increasing concentration of Bacterial MVs correlating with the increased fluidity of host model membrane. **(I)** Fluorescence intensity ratio at 420/520 nm of wavelength and dipole potential of the outer leaflet model membrane incubated with increasing concentration of Bacterial MVs, increased at high concentration of Bacterial MVs. (**J**) Surface Pressure (π) - Mean molecular area (A) isotherm of OLMM monolayer (black curve) and OLMM incubated with bacterial MVs (red curve) showing right shift. All isotherms were compressed with constant speed of 8 mm/minute at 25 °C temperature. (**K**) Compressibility modulus (in-plane elasticity, C_s^{-1}) with respect to surface pressure of OLMM monolayer (black curve) and OLMM with MV (red curve) showing decreased C_s^{-1} on the air-water interface. (**L**) Excess Gibb's free energy of mixing between OLMM and bacterial MVs shows an ideal mixing and decrease with increasing surface pressure calculated from Langmuir isotherms. All fluorescence spectroscopic data are shown as mean ± S.E. from three independent experiments. Significant variations were compared through one-sided ANOVA of OLMM treated with 0.2 mg/mL and 0.6 mg/mL of Bacterial MVs with respect to control, where,

bioRxiv preprint doi: https://doi.org/10.1101/827519; this version posted November 2, 2019. The copyright holder for this preprint (which was not certified by peer review) is the author/funder. All rights reserved. No reuse allowed without permission.

(***) depicts p<0.001, (**) p<0.01 and (*) p<0.05, data point with no asterisk mark are not significant. All representative isotherms are the mean of independently performed experiments. For isotherms and compressibility modulus curves the estimated standard error for data points of surface pressure (π) with respect to area per molecule (A) was approximately ±0.05 mN/m.

Previous investigations have reported that Bacterial MVs can not only associate with the host cell surfaces but also incorporate with different phospholipid liposomes in vitro[10]. However, an important caveat that remains unclear is the lipid specificity of the MV interaction and how it may modulate the host cell membrane parameters. Irrespective of the kind of bacterial MV, the interaction with the host lipid membrane takes place between the outer membrane of the bacterial MVs and the host membrane. To this end, we reconstituted giant unilamellar vesicles (GUVs) comprising of the outer leaflet lipids of a eukaryotic cells (i.e., DOPC 35 mole %, DOPE 5 mole %, Brain SM 20 %, Cholesterol 30 %), in order to mimic the host cell membrane [13]. To visualize the interaction of bacterial MVs, we labeled GUVs with Rhodamine-PE (emission wavelength, red) and bacterial MVs with DiO (emission wavelength, green). Confocal microscopy revealed the binding of bacterial MVs with the outer leaflet model membranes (OLMM) (Figure 1G). The kinetics of binding of bacterial MVs to the host membrane comprising outer leaflet lipids appeared to be fast as reported earlier in different cell lines[14]. We next sought to investigate whether the interaction of the bacterial MVs with the host membrane results in changes in the fluidity and dipole potential of the host membrane. The changes in membrane fluidity were quantified by reconstituting a potentiometric styryl membrane probe di-8-ANEPPS (Pyridinium, 4-[2-[6-(dioctylamino)-2-naphthalenyl]ethenyl]-1-(3-sulfopropyl)), with membrane vesicles, whose fluorescence anisotropy (a measure of rotational relaxation time) responds to the changes in the dynamics of the membrane environment. The fluorescence anisotropy of the host outer leaflet model membrane was found to decrease by ~ 9 % upon MV interaction suggesting increased fluidization of the host membrane (Figure 1H). Likewise, the probe di-8-ANEPPS, is known to undergo shift in the fluorescence excitation spectrum in linear response to dipole potential changes in the lipid environment, which in turn, is dependent on the electric field in the membrane environment [15-17]. The dipole potential originates from the non-random arrangement of molecular dipoles (i.e., water, carbonyl-groups and lipid head-groups) at the membrane

bioRxiv preprint doi: https://doi.org/10.1101/827519; this version posted November 2, 2019. The copyright holder for this preprint (which was not certified by peer review) is the author/funder. All rights reserved. No reuse allowed without permission.

interface [18]. The dipole potential of the host outer leaflet model membrane was found to increase by ~ 67 % upon the interaction of MV suggesting strong interaction (Figure 1I). Further, the surface zeta potential of the bacterial MVs was found to be ~ - 9 mV and that of the outer leaflet model membrane lipid components was also found to be negative, however, of higher magnitude (- 20mV to - 25mV) as compared to bacterial MVs (table S1).

Bacterial MV fusion increases the elasticity and facilitates bending of host model membrane

After identifying the lipid specificity of MV interaction and estimating the accompanied changes in the fluidity and dipole potential of the host membranes, we further sought to quantify the observed changes at a molecular level. Langmuir monolayer surface area-pressure isotherms are a powerful means that enable quantification of the thermodynamic aspects of the MV interaction with the host model membranes and the associated changes in physicochemical properties of the host membranes [18]. Further, the variation of compositional parameters mimicking the biological conditions in monolayer experiments allows to dissect the contribution/modulation of hydrophobic interactions, charges, dipole potential during the MV-host membrane interaction.

We first investigated the surface pressure-area (-*A*) isotherms for the outer leaflet model membrane (OLMM). OLMM being a complex multi-component lipid mixture only showed liquid-expanded (L_e) and -condensed (L_c) behaviour, without any significantly evident 2D phase transition (Figure 1J). Marked increase in the area per molecule with increasing surface pressure was observed, in the presence of MV in the sub-phase suggesting significant interaction and fusion between the monolayer membrane and bacterial MVs (Figure 1J). To further corroborate our conclusions, the changes in the host model membrane surface compressional modulus, C_s^{-1} (i.e., reciprocal of surface compressibility or elasticity, C_s), were extracted using the slopes obtained from (-*A*) isotherms. Compressibility modulus, C_s^{-1}, is related to the change in surface pressure and area per molecule, as defined in equation (1) -

$$C_s^{-1} = -A\frac{d\pi}{dA} \qquad (1)$$

bioRxiv preprint doi: https://doi.org/10.1101/827519; this version posted November 2, 2019. The copyright holder for this preprint (which was not certified by peer review) is the author/funder. All rights reserved. No reuse allowed without permission.

and is known to be very sensitive to subtle changes in lipid structure during lateral interaction and thus, provides molecular insights into lateral packing elasticity of the host membrane [19-21]. Upon the fusion of bacterial MVs, the monolayer compressibility modulus was found to have decreased by ~ 7mN/m (Figure 1K), particularly nearing a surface pressure of 30-35 mN/m which has been established to possess identical chemical potential and molecular area to that of bilayers in equilibrium [22]. Further, the excess Gibbs free energy of mixing of bacterial MVs with OLMM was calculated at certain surface pressures by integrating the excess area over surface pressure, and denoted by the equation [23] (2):

$$\Delta G_{Excess} = \int_0^{\pi} [\, A_{12} - (X_1 A_1 + X_2 A_2)] \, d\pi \qquad (2)$$

where, A_{12} is the mean molecular area occupied by the mixed monolayer in the presence of MV, A_1 and A_2 are the mean molecular areas occupied by monolayer and bacterial MVs respectively, and X_1 and X_2 are the molar fractions of the monolayer component and bacterial MVs respectively. ΔG_{Excess} showed a decrease with increasing surface pressure suggesting the mixing of MV with monolayer lipids to be more favourable till a surface pressure at 10 mN/m whereas slight increase was observed at 15 mN/m and 20mN/m (Figure 1L), as the maximum crowding of bacterial MVs approached as reflected in the (Figure S2). The difference of the collapse pressures (π_c) of monolayer membranes in the presence and absence of MV depicts the change in bending force (ΔF_b) acting on the monolayer during the adhesion which was calculated using the equation (3):

$$\Delta F_b = MM.MV\pi_c - MM\pi_c \qquad (3)$$

where, $MM.MV\pi_c$ is the collapse pressure of model membrane with bacterial MVs in subphase and $MM\pi_c$ being without bacterial MVs. Negative values of (ΔF_b) suggest bending of monolayer [24]. The (ΔF_b) was found to be ~ -1.75 mN/m suggesting the feasibility of bending upon adhesion of bacterial MVs (table S2). Highest surface pressure of 20.95 mN/m was taken in each case as it is the collapse pressure of MV components monolayer (Figure S2). In addition, we also examined the *-A* isotherms of the MV components (i.e., lipopolysaccharides, phospholipids devoid of any proteins)

bioRxiv preprint doi: https://doi.org/10.1101/827519; this version posted November 2, 2019. The copyright holder for this preprint (which was not certified by peer review) is the author/funder. All rights reserved. No reuse allowed without permission.

extracted from bacterial MVs (see methods for biphasic solvent extraction). A clear gaseous phase was observed in the beginning followed by L_e phase and a short L_c phase just before the collapse at around 21mN/m (Figure S2). The compressibility modulus showed a sharp rise till a surface pressure of 2-3mN/m from which it became constant at a value of 16mN/m. Both lower collapse pressure and constant compressibility modulus suggest a significantly rigid behaviour resisting compression (Figure S2).

Role of host membrane lipid head group in bacterial MV interaction

We next questioned if there is any lipid specific preferential interaction of the bacterial MVs with the host cell membrane outer leaflet that majorly contributes towards interaction/fusion of bacterial MVs. To probe this, we reconstituted liposomes composed of the major phospholipids present in the outer leaflet of the host cell membrane i.e., DOPC, DOPG, BSM and Liver PI. We analyzed the binding and colocalization of bacterial MVs with lipid membranes i.e. DOPC, DOPG and Liver PI, to visualize lipid-bacterial MVs interaction (Figure 2A, 2D and 2G). Significant binding of bacterial MVs to all the above lipid membranes was observed as evident from the homogenous DiO signal (*green*) arising from the equatorial plane of giant unilamellar vesicels (GUVs) colocalizing with Rhodamine PE signal (*red*). After confirming the interaction of bacterial MVs with DOPC, DOPG and Liver PI lipids, we further quantified the modulation of fluidity and dipole potential changes in these lipid membranes. We found that DOPC, DOPG, BSM and Liver PI membranes, all undergo significant changes in the membrane fluidity upon the interaction of bacterial MVs. Interestingly, the fluorescence anisotropy of the dye was found to decrease in case of DOPC, DOPG and Liver PI by ~ 66 %, 45 % and 45 % respectively, suggesting enhanced fluidization (Figure 2B, 2E and 2H). On the contrary, the membrane composed of BSM showed an increase in the fluorescence anisotropy of the dye by 7 %, suggesting the membrane becoming more rigid (Figure S3). We then investigated the role of lipid head group on the MV induced dipole potential changes in the host membrane. We observed that membranes composed of DOPC, DOPG and Liver PI undergo significant changes in their dipole potential (i.e., 21 %, 15 % and 9 % respectively) (Figure 2C, 2F, and 2I). On the contrary, membranes composed of BSM did not undergo any significant change in the measured dipole potential (Figure S3).

bioRxiv preprint doi: https://doi.org/10.1101/827519; this version posted November 2, 2019. The copyright holder for this preprint (which was not certified by peer review) is the author/funder. All rights reserved. No reuse allowed without permission.

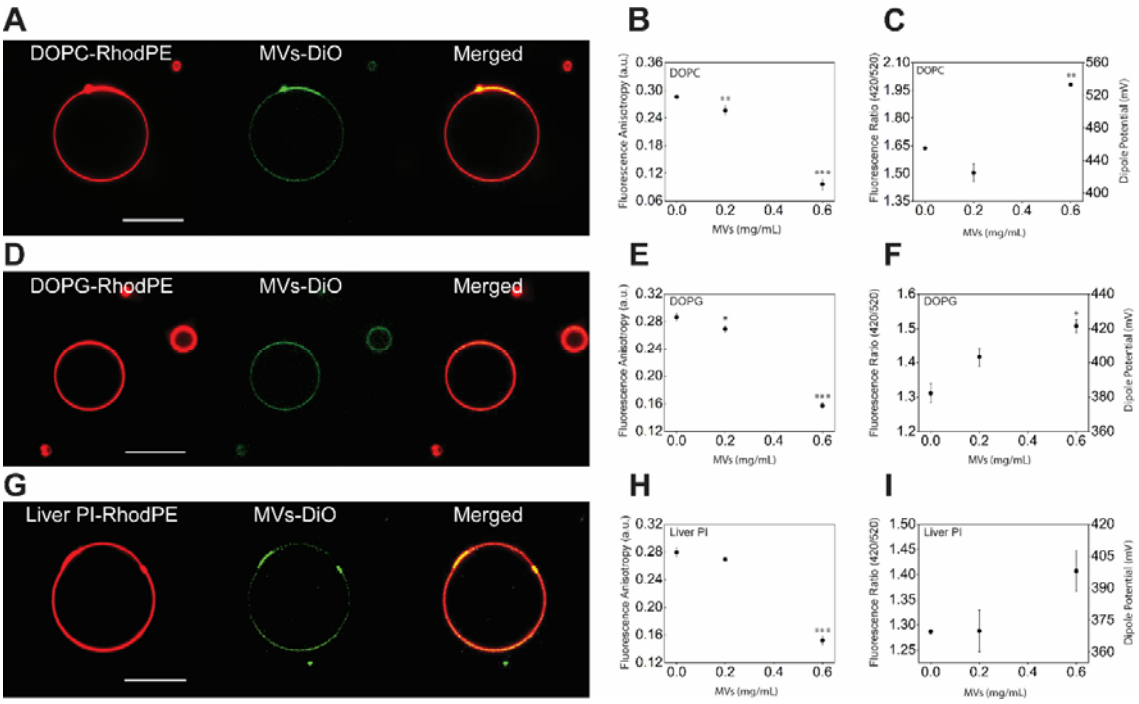

Figure 2. Monitoring the lipid specificity of host membrane for bacterial MVs interaction using confocal and the fluorometry of the potentiometric dye, Di-8-ANEPPS. (A) Fluorescence image of DOPC doped with 1% Rhodamine PE (*red fluorescence)* mixed with bacterial MVs labelled with DiO (*green fluorescence)* to visualize the interaction of bacterial MVs with lipid membrane. A green fluorescence signal on the equatorial plane of DOPC membrane suggests the interaction of bacterial MVs with DOPC phospholipid. **(B)** Membrane fluidity of DOPC decreased with increasing concentration of bacterial MVs i.e. 0 mg/mL, 0.2 mg/mL and 0.6 mg/mL. **(C)** Fluorescence ratio 420/520 nm and dipole potential (mV) increased for DOPC membrane at 0.6 mg/mL concentration of bacterial MVs with respect to control DOPC membrane. **(D)** Fluorescence image of DOPG doped with 1% Rhodamine PE (*red fluorescence)* mixed with bacterial MVs labelled with DiO (*green fluorescence)* to visualize the interaction of bacterial MVs with lipid membrane. A green fluorescence on the equatorial plane of DOPG membrane suggests the interaction of bacterial MVs with DOPG phospholipid. **(E)** Anisotropy of DOPG decreased with increasing concentration of bacterial MVs. **(F)** Dipole potential of DOPG membrane increased linearly with increasing concentration of bacterial MVs. **(G)** Fluorescence image of Liver PI doped with 1% Rhodamine PE (*red fluorescence)* mixed with bacterial MVs labelled with DiO (*green fluorescence)* to visualize the interaction of bacterial MVs with lipid membrane. A

bioRxiv preprint doi: https://doi.org/10.1101/827519; this version posted November 2, 2019. The copyright holder for this preprint (which was not certified by peer review) is the author/funder. All rights reserved. No reuse allowed without permission.

green fluorescence on the equatorial plane of Liver PI membrane suggests the interaction of MVs with Liver PI phospholipid. **(H)** Liver PI membrane shows increase in fluidity with MVs treatment as compared to control. **(I)** Dipole potential of Liver PI had increase at 0.6 mg/mL of MVs whereas it remained unchanged at lower concentration i.e. 0.2 mg/mL. Measurements for calculation of dipole potential were done at measured intensity at excitation wavelength set at 420 and 520 nm respectively. All fluorescence spectroscopic data are shown as mean ± S.E. from three independent experiments. Significant variations were compared through one-sided ANOVA of membrane condition treated with Bacterial MVs with respect to control (only lipid membrane without Bacterial MVs), where, (***) depicts $p<0.001$, (**) $p<0.01$ and (*) $p<0.05$, test data point) with no asterisk mark are non-significant.

We then sought to investigate the modulation of membrane elasticity upon MV fusion and mixing with regard to various lipid head-groups. We observed, MV addition caused decrease in area per molecule in case of DOPC, whereas only slight change in Liver PI, which remained almost constant with increasing pressure (Figure 3A and 3C). Coexistence of L_c+L_e phase seemed to be very mild in DOPC curve with no clear occurrence in the other two lipids. On the contrary, an increase in the molecular area of DOPG in the presence of MV was observed as evident in the rise in surface pressure (Figure 3B). A reduction of 1.52 mN/m and 3.01 mN/m in the collapse pressure of DOPC and Liver PI membrane was observed, though DOPG membrane showed a little rise of 0.72 mN/m (Figure 3A-3C). The negative values of the change in bending force () suggest bending of monolayer [24] by the interacting MV as observed in case of both DOPC and Liver PI lipid membranes (Figure 3H). Further, MV interaction/fusion induced a reduction in monolayer compressibility modulus (C_s^{-1}) by around ~ 25 mN/m, ~ 2 mN/m and ~ 15 mN/m, in DOPC, DOPG and Liver PI lipid membranes, respectively. (Figure 3D, 3E and 3F). The reduction in C_s^{-1} in the presence of MV suggests a rise in the membrane monolayer compressibility. We next wanted to see if the mixing of MV with each lipid monolayer is thermodynamically favourable or not. A decreasing negative value trend in ΔG_{Excess} was observed (Figure 3G) with respect to increasing surface pressure till 15 mN/m in DOPC and Liver PI and 10 mN/m in DOPG after which the curve rose. Upon the mixing of MV, DOPG membrane monolayer showed the lowest free energy change of ~ -1.05 kJ/mol and highest being ~ -1.7 kJ/mol for Liver PI indicating more favourable mixing with Liver PI monolayer.

bioRxiv preprint doi: https://doi.org/10.1101/827519; this version posted November 2, 2019. The copyright holder for this preprint (which was not certified by peer review) is the author/funder. All rights reserved. No reuse allowed without permission.

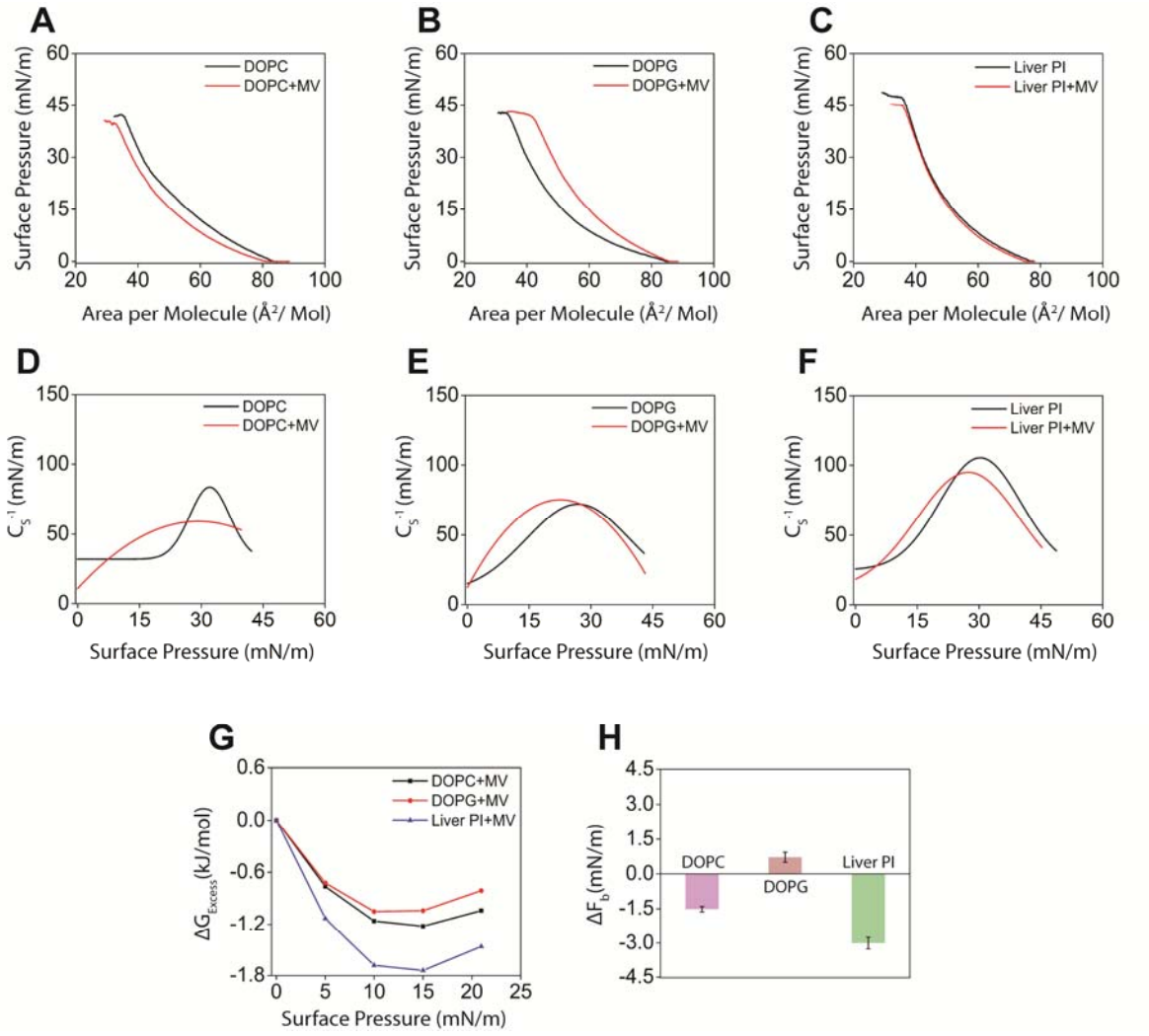

Figure 3. Surface Pressure (π)-mean molecular area (A) isotherms, changes in compressibility modulus, excess free energy change and changes in bending force rigidity of different headgroup containing phospholipid monolayers at air-water interface with and without bacterial MVs in the subphase. π-A isotherms of **(A)** DOPC, **(B)** DOPG and **(C)** Liver PI with and without bacterial MVs obtained at 25°C. Variations in the compressibility modulus as a function of surface pressure acquired for **(D)** DOPC, **(E)** DOPG and **(F)** Liver PI with and without bacterial MVs from respective Langmuir isotherms. **(G)** Variation in the excess Gibb's free energy of mixing of bacterial MVs at surface pressures 0 mN/m, 5 mN/m, 10 mN/m, 15mN/m and 20.95 mN/m with DOPC, DOPG and Liver PI monolayers at the interface. **(H)** Histogram

bioRxiv preprint doi: https://doi.org/10.1101/827519; this version posted November 2, 2019. The copyright holder for this preprint (which was not certified by peer review) is the author/funder. All rights reserved. No reuse allowed without permission.

depicting change in bending force (ΔF_b) of DOPC, DOPG and Liver PI monolayers at the interface in presence of bacterial MVs. All isotherms were recorded at a constant barrier compression speed of 8 mm/min at 25°C temperature. All representative isotherms are the mean of independently performed experiments. For isotherms and compressibility modulus curves the estimated standard error for data points of surface pressure (π) with respect to area per molecule (A) was approximately ±0.05 mN/m

Role of host membrane lipid acyl chain length in bacterial MV interaction

The lipid acyl chain length is known to determine the membrane bilayer thickness as well as contributes to the degree of fluidity of the membranes [25]. Therefore, we then sought to investigate the role of lipid acyl chain (i.e., C12, C14, C16, C18) of host membrane in the MV mediated changes in the overall host membrane fluidity and dipole potential. The overall fluorescence anisotropy of the dye was found to decrease by ~ 30 % in DPPC suggesting increased fluidization (Figure 4C), and increase by ~ 28 %, ~ 43 % and ~ 27 % in DLPC, DMPC and DSPC respectively, suggesting decrease in fluidity (Figure 4A, 4B and 4D). The contrasting observation is noteworthy, as it suggests, that MV interaction seems to enhance the fluidity of a relatively less fluid membrane (such as DPPC, C16) and decrease the fluidity of relatively more fluid membranes (such as C12,14). The observed fluctuations in the fluorescence anisotropy with increasing concentrations of the MV, could hint at a dynamic interaction during the crowding/interaction of the MV. Further, the dipole potential was found to increase in all cases (DMPC, DPPC and DSPC) but decrease in DLPC membranes upon MV interaction (Figure 4E-4H). In case of DMPC (Figure 4F) and DSPC (Figure 4H) in highest concentration the dipole potential was increased to ~ 30% and ~ 15% respectively, as compared to control which confirms interaction of bacterial MVs with DMPC and DSPC membrane. Likewise, DPPC membrane shows significant increase in dipole potential upon interaction with MV (Figure 4G). On the contrary, MV interaction with DLPC membranes resulted in less significant change in the dipole potential (Figure 4E).

bioRxiv preprint doi: https://doi.org/10.1101/827519; this version posted November 2, 2019. The copyright holder for this preprint (which was not certified by peer review) is the author/funder. All rights reserved. No reuse allowed without permission.

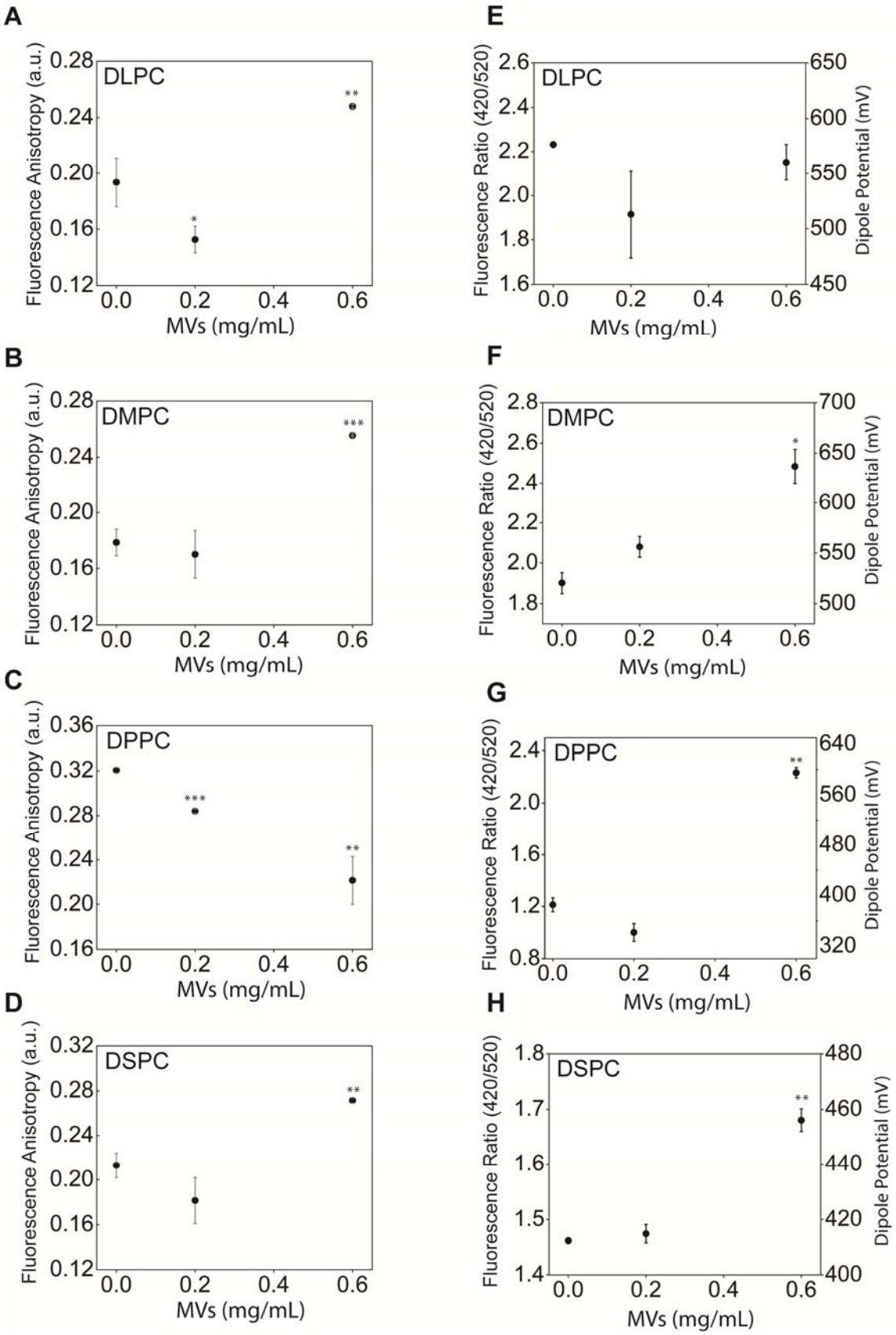

bioRxiv preprint doi: https://doi.org/10.1101/827519; this version posted November 2, 2019. The copyright holder for this preprint (which was not certified by peer review) is the author/funder. All rights reserved. No reuse allowed without permission.

Figure 4. Variation in anisotropy and dipole potential of phospholipids with increasing bilayer thickness as a function of acyl chain length, treated with OMVs. Fluorescence anisotropy of individual lipid model membranes (**A**) DLPC, (**B**) DMPC, (**C**) DPPC, and (**D**) DSPC incubated with increasing concentration of OMVs. Changes in fluorescence ratio and dipole potential of (**E**) DLPC, (**F**) DMPC, (**G**) DPPC, and (**H**) DSPC membrane with respect to increasing concentrations of OMVs i.e. 0 mg/mL, 0.2 mg/mL and 0.6 mg/mL. All fluorescence spectroscopic data are shown as mean ± S.E. from three independent experiments. Significant variations were compared through one-sided ANOVA of membrane condition treated with OMVs with respect to control (only lipid membrane without OMVs), where, (***) depicts $p<0.001$, (**) $p<0.01$ and (*) $p<0.05$, data point with no asterisk mark are non-significant.

We then sought to question the role of lipid acyl chain length in MV interaction/fusion using monolayer of lipids at the air-water interface. This is important as under cellular conditions transient phase separated regions differ in the membrane thickness[25]. To investigate the role of chain length we have chosen zwitterionic headgroup with phophatidylcholine having varying chain length which were DLPC, DMPC, DPPC and DSPC lipids (i.e., C12:0, C14:0, C16:0 and C18:0, respectively). The -A isotherms of the monolayers having lipids of various chain length formed at 25°C treated with bacterial MVs is shown in Figure 5A-5D. Analysis of surface pressure-area curves of monolayers of increasing acyl chain length, which corresponds to membrane bilayer thickness, were in good agreement with previous reports [26]. We observed that the mean molecular area occupied by phospholipids decrease with increasing chain length in control conditions except DPPC i.e. in absence of bacterial MVs (Figure 5A-5D), which can be explained by the effective acyl chain hydrophobic interactions[27]. In presence of bacterial MVs, increase in area per molecule was observed in each of the four membrane monolayers with rise in surface pressure (Figure 5A-5D). The observed increase in molecular area was fairly constant throughout all the phases in DLPC, DPPC and DSPC membrane monolayers (Figure 5A, 5C and 5D) whereas an increasing trend was observed in DMPC till 15 mN/m (Figure 5B). Decrease in collapse pressure by 3.15 mN/m and 5.04 mN/m was calculated for DLPC and DMPC. Highest decrease in collapse pressure of ~ -7 mN/m amongst all lipids was observed for DPPC after MV addition suggests most significant bending of membrane in 16:0 acyl chain length. This decline was least in case of DSPC (Figure 5J). Figure 5E-5H show monolayer compressibility curves of the

bioRxiv preprint doi: https://doi.org/10.1101/827519; this version posted November 2, 2019. The copyright holder for this preprint (which was not certified by peer review) is the author/funder. All rights reserved. No reuse allowed without permission.

lipids in presence of MV with respect to control. A fall in compressibility modulus by around 10 mN/m was seen in DLPC, whereas the same decline was 35 mN/m in DPPC. Compressibility modulus showed a dramatic increase in case of DMPC and DSPC with a value of almost 50 mN/m and 60 mN/m. The ΔG_{Excess} change though followed falling trend up to a particular pressure, there was not much difference between the energy curves of individual lipids (Figure 5I). At 15 mN/m, the free energy change was highest in DLPC followed by DPPC suggesting ideal mixing of bacterial MVs with these membranes. The lowest energy change of mixing was observed in case of DMPC throughout all pressures (Figure 5I).

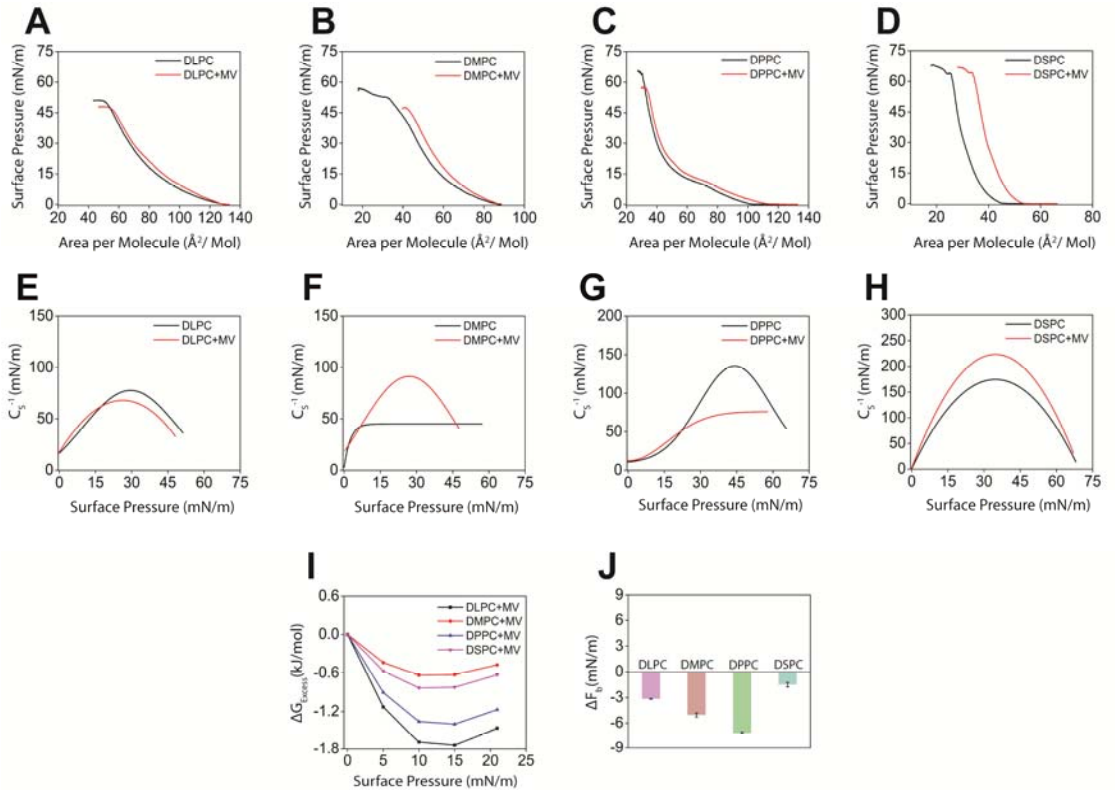

Figure 5. Surface Pressure (π)-mean molecular area (A) isotherm of monolayers composed of phospholipids with increasing acyl chain length at air-water interface with (Red curve) and without (Black curve) OMVs in the subphase. π-A isotherms of (**A**) DLPC (12:0), (**B**) DMPC (14:0), (**C**) DPPC (16:0) and (**D**) DSPC (18:0) with and without OMVs obtained at 25°C. Changes in compressibility modulus plotted as a function of surface pressure acquired for (**E**) DLPC, (**F**) DMPC, (**G**) DPPC and (**H**) DSPC without and with OMVs, from respective Langmuir isotherms. (**I**) Variation in the excess Gibb's free of mixing of OMVs at surface pressures 0 mN/m, 5 mN/m, 10 mN/m, 15mN/m and 20.95 mN/m with DLPC, DMPC, DPPC and DSPC monolayers at

bioRxiv preprint doi: https://doi.org/10.1101/827519; this version posted November 2, 2019. The copyright holder for this preprint (which was not certified by peer review) is the author/funder. All rights reserved. No reuse allowed without permission.

interface. (**J**) Histogram showing change in bending force (ΔF_b) of DLPC, DMPC, DPPC, and DSPC monolayers at the interface in presence of OMVs All isotherms were recorded at a constant barrier compression speed of 8 mm/min at 25°C. All representative isotherms are the mean of independently performed experiments. For isotherms and compressibility modulus curves the estimated standard error for data points of surface pressure (π) with respect to area per molecule (A) was approximately ±0.05 mN/m.

Lipid Membrane Rigidity and Phase Separation Modulate MV Fusion

Host cell membranes are multi-component lipid assembly that is a non-equilibrium homogenous system close to phase separation. The membrane environment has highly transient phase separating regions called rafts important for cellular signaling. We therefore investigated the effect of phase behaviour on the interaction of the bacterial MVs. In order to probe this, we reconstituted liposomes (GUVs and LUVs) made of widely accepted ternary membrane composition (i.e., DOPC:BSM:Cholesterol) and varied the amounts of cholesterol to enable different degrees of liquid-disordered (L_d) and liquid-ordered (L_o) regions. This would mimic the biologically relevant highly dynamic local changes in membrane phase boundaries[28]. First, we reconstituted GUVs composed of DOPC/BSM without any cholesterol representing a fully disordered (L_d) phase in membrane to examine how the L_d forming membrane condition effects the interaction of MV (*liquid disordered; DOPC:BSM:Chol 5:5:0*). Uniform adhesion/fusion of bacterial MVs to the fully disordered membrane was observed. We arrived at this conclusion by monitoring all the planes of stacks as well as 3D-stack image of GUV incubated with bacterial MVs (Figure 6A). The fluorescence anisotropy of the dye increased by 30% upon interaction with MV in a concentration dependent manner indicating decrease in membrane fluidity (Figure 6B). Further, the membrane dipole potential was found to linearly decrease upon the interaction of MV (Figure 6C), all of which hint at binding of bacterial MVs that may allow some lipid mixing [29].

We then modulated the degree of phase separation, which in turn effects the line tension at the phase separating boundaries [30], by reconstituting membranes having L_o/L_d phase separated regions by changing the cholesterol levels (i.e, *DOPC:BSM:Chol, 4:4:2/3:3:4*). Interestingly, in case of L_o/L_d phase separating membranes with moderate

bioRxiv preprint doi: https://doi.org/10.1101/827519; this version posted November 2, 2019. The copyright holder for this preprint (which was not certified by peer review) is the author/funder. All rights reserved. No reuse allowed without permission.

levels of cholesterol (*DOPC:BSM:Chol, 4:4:2*) significant binding of bacterial MVs was observed (Figure 6D). The fluidity decreased in a similar manner as for the L_o membrane as reflected in the increase fluorescence anisotropy of the dye by 15 % (Figure 6E). Similarly, the dipole potential was found to linearly decrease upon the interaction of MV (Figure 6F). Interestingly, in case of phase separating membranes comprising higher amount of cholesterol (*DOPC:BSM:Chol, 3:3:4*), having a larger L_o (liquid ordered) regions the MV binding was found to be relatively weak (Figure 6G). Also, the fluidity was found to decrease as in earlier cases, however, without any change in the dipole potential of the membrane (Figure 6H and 6I).

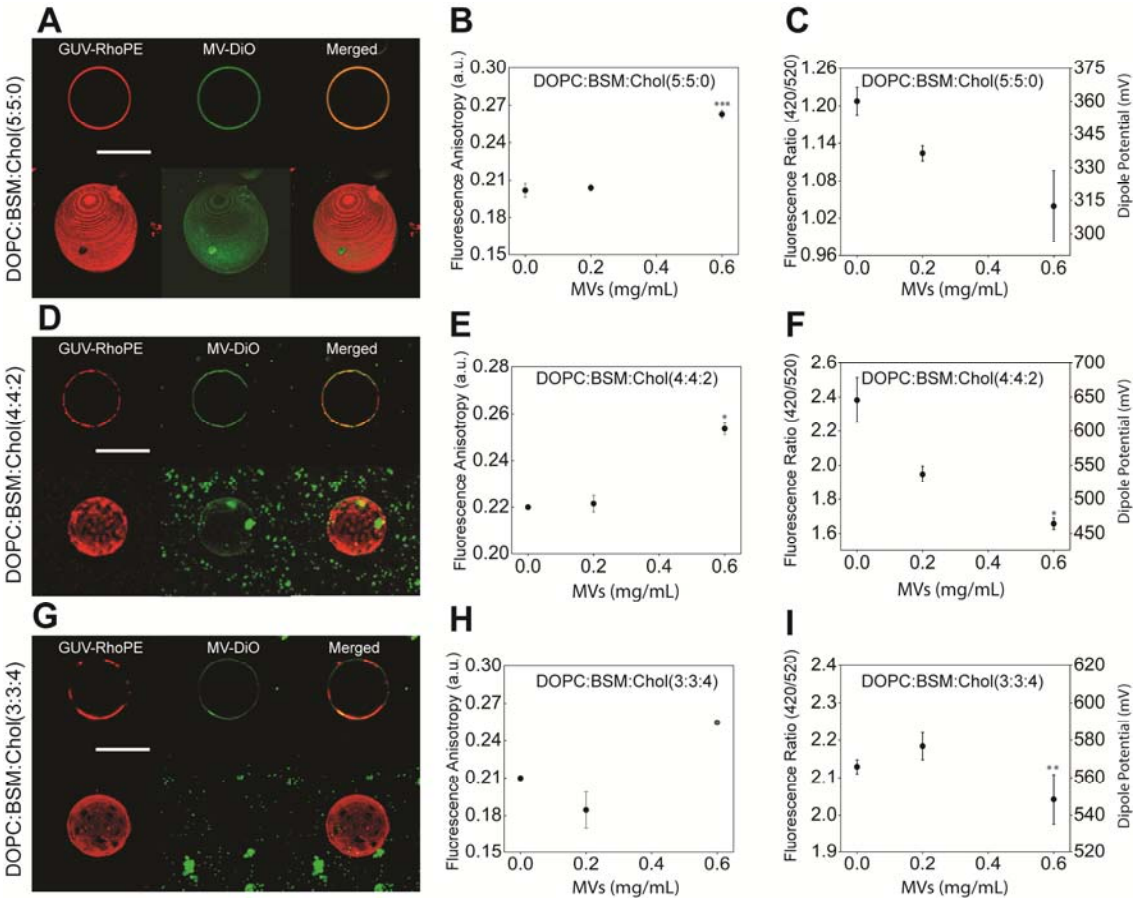

Figure 6. Effect of increasing concentration of cholesterol (liquid order) and phase behaviour of membrane on binding, changes in membrane fluidity and membrane dipole potential treated with bacterial MVs. (A) Fluorescence image showing GUVs composed of DOPC:BSM:Chol in the molar ratio of 5:5:0 doped with 1 mole % Rhodamine PE (*red channel)* interaction with DiO labelled bacterial MVs *(green channel)*. Bacterial MVs distribution on equatorial plane of GUVs is represented by merged image of both red and green channels along with the 3D stack of each channel.

bioRxiv preprint doi: https://doi.org/10.1101/827519; this version posted November 2, 2019. The copyright holder for this preprint (which was not certified by peer review) is the author/funder. All rights reserved. No reuse allowed without permission.

(B) Fluorescence anisotropy of fully disordered DOPC:BSM:Chol 5:5:0 membrane induced by bacterial MVs, **(C)** Dipole potential of fully disordered (DOPC:BSM:Chol 5:5:0) treated with increasing concentration of bacterial MVs. **(D)** Multiple lipid domain can confine the binding of bacterial MVs to partially disordered DOPC:BSM:Chol 4:4:2 membrane (*left*- Rhodamine PE- (red), *centre*- DiO (green) and *right*- merged). Top panel is showing MV binding to equatorial plane of GUVs and the panel below is bacterial MVs 3D-stack of GUV-MVs mixture. **(E)** Membrane fluidity variation in DOPC:BSM:Chol in molar ratio of 4:4:2 membrane treated with bacterial MVs in increasing concentration. **(F)** Dipole potential of (DOPC:BSM:Chol) in mole ratio of 4:4:2 treated with bacterial MVs in increasing concentration. **(G)** Fluorescence image showing GUVs composed of DOPC:BSM:Chol in the molar ratio of 3:3:4 correspond to liquid ordered domain (l_o) doped with 1 mole % Rhodamine PE (*red channel)* interaction with DiO labelled MVs *(green channel)*. bacterial MVs has least binding with DOPC:BSM:Chol; 3:3:4 represented by merged image of both red and green channels along with the 3D stack of each channel. **(H)** Changes in anisotropy of DOPC:BSM:Chol (3:3:4) treated with increasing concentration of bacterial MVs. **(I)** Fluorescence ratio and dipole potential of (DOPC:BSM:Chol 3:3:4) treated with increasing concentration of Bacterial MVs. At least 30 GUVS visualized under microscope and scale bar is 10 µM. All fluorescence spectroscopic data are shown as mean ± S.E. from three independent experiments. Significant variations were compared through one-sided ANOVA of membrane condition treated with bacterial MVs with respect to control (only lipid membrane without bacterial MVs), where, (***) depicts $p<0.001$, (**) $p<0.01$ and (*) $p<0.05$, test data point (membrane treated with bacterial MVs) with no asterisk mark are non-significant.

We then investigated the role of cholesterol in bacterial MV interaction/fusion and the subsequent mechano-elastic changes in lipid monolayer. To this end, as described earlier we used different concentrations of cholesterol to make ternary lipid mix containing *DOPC:BSM:Chol* in 5:5:0, 4:4:2 and 3:3:4 ratio, mimicking membranes with fully disordered (*5:5:0*) and co-existing phase separated regions (*4:4:2 and 3:3:4*). π *-A* isotherms of show similar trend with increase in molecular area in the presence of MV (Figure 7A-7C). A noticeable aspect observed in the monolayer with highest cholesterol content (3:3:4) in the presence of MV, was that - after surface pressure of around 7.5 mN/m, there was a left shift followed by a right shift after 35 mN/m. Collapse pressure

bioRxiv preprint doi: https://doi.org/10.1101/827519; this version posted November 2, 2019. The copyright holder for this preprint (which was not certified by peer review) is the author/funder. All rights reserved. No reuse allowed without permission.

reduced in 0% and 40% cholesterol concentration while increased by 0.44 mN/m in the case of 20% (Figure 7H). Compressibility modulus (Figure 7D-7F) clearly show how increasing concentration of cholesterol induces decrease in monolayer elasticity after MV adhesion, the highest being in case of 40% cholesterol. ΔG_{Excess} was significantly high in case of 4:4:2 as compared to the other two mixtures at all pressures.

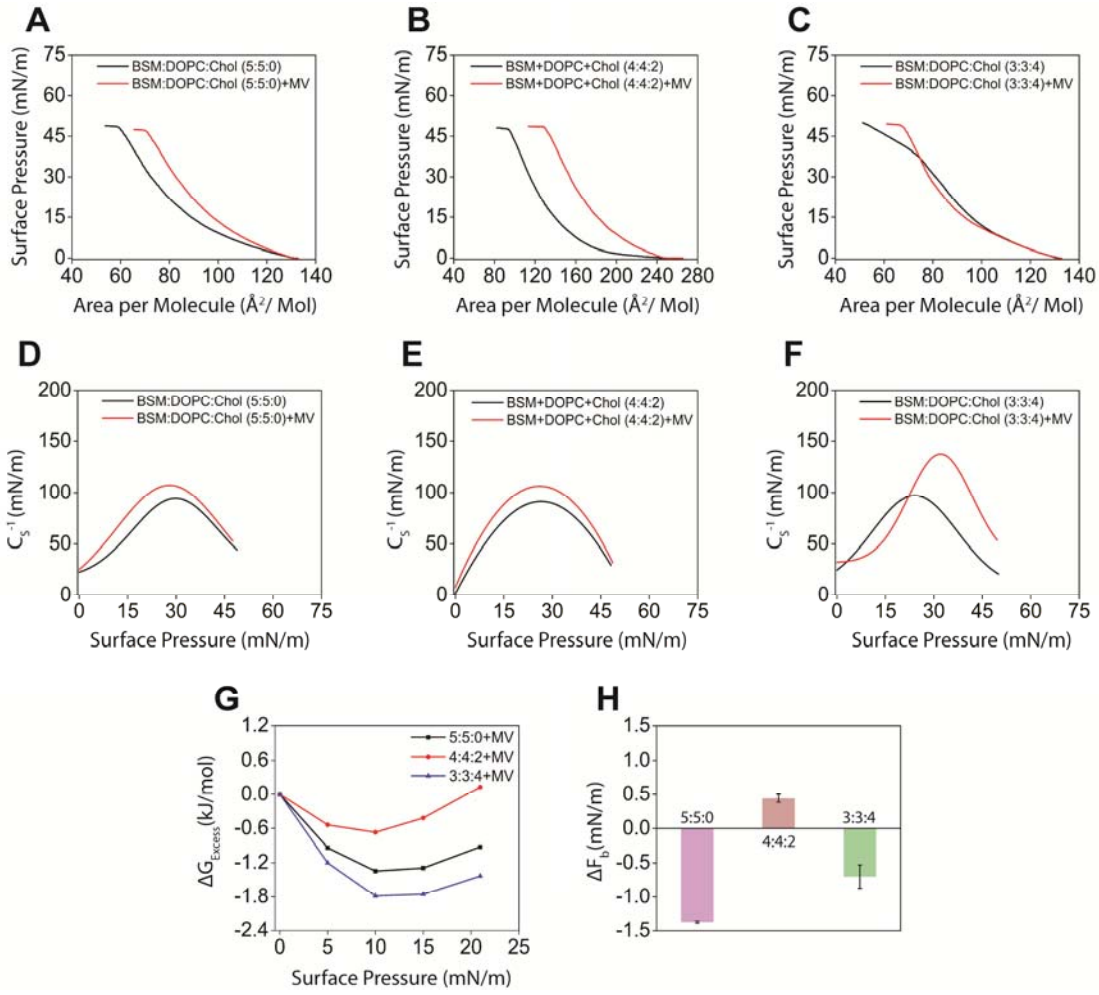

Figure 7. Surface Pressure (π)-mean molecular area (A) isotherm of monolayers having varying cholesterol concentration at air-buffer interface with (Red curve) and without (Black curve) bacterial MVs in the subphase. π-A isotherms of **(A)** 5:5:0 (BSM:DOPC:cholesterol), **(B)** 4:4:2 (BSM:DOPC: cholesterol) and **(C)** 3:3:4 (BSM:DOPC:cholesterol) with and without bacterial MVs obtained at 25°C. Variability in compressibility modulus plotted as a function of surface pressure acquired for **(D)** 5:5:0, **(E)** 4:4:2 and **(F)** 3:3:4 from respective Langmuir isotherms. **(G)** Variation of excess Gibb's free energy of mixing of bacterial MVs with lipid monolayer as a function of increasing surface pressures 0 mN/m, 5 mN/m, 10 mN/m, 15 mN/m and 20.95 mN/m.

bioRxiv preprint doi: https://doi.org/10.1101/827519; this version posted November 2, 2019. The copyright holder for this preprint (which was not certified by peer review) is the author/funder. All rights reserved. No reuse allowed without permission.

(H) Bending force (ΔF_b) histogram of 5:5:0, 4:4:2 and 3:3:4 monolayers at the interface in presence of bacterial MVs. All isotherms were recorded with constant barrier compression speed of 8 mm/min at 25°C. All representative isotherms are the mean of independently performed experiments. For isotherms and compressibility modulus curves the estimated standard error for data points of surface pressure (π) with respect to area per molecule (A) was approximately ±0.05 mN/m.

bioRxiv preprint doi: https://doi.org/10.1101/827519; this version posted November 2, 2019. The copyright holder for this preprint (which was not certified by peer review) is the author/funder. All rights reserved. No reuse allowed without permission.

Discussion

Despite the different physicochemical architecture of the bacterial MVs and the eukaryotic host cell membranes, membrane fusion is accepted as one of the mechanisms of MV entry [3, 11]. In this study we reconstitute the MV interaction with GUVs and monolayer membranes mimicking various host cellular membrane conditions to quantitatively elucidate the MV mediated modulation of host membrane properties such as fluidity, dipole potential and elasticity. To do this, a non-pathogenic *E. coli* strain was chosen as a model Gram-negative bacteria to isolate bacterial MVs. The bacterial MVs labelled with Nile Red was found to undergo significant internalization by macrophage and fusion with liposomes (Figure 1F), in line with previous observations [10]. Fusion of bacterial MVs to host membranes is involved in transmission of virulence factors in non-phagocytic cells [14] as well as in reprogramming of phagosomes in phagocytic macrophage [31, 32]. The homogenous binding of DiO-labelled bacterial MVs (*green*) to the reconstituted lipid membranes (*Rhodamine-PE labelled, red*) mimicking the outer-leaflet of the host cell membrane (Figure 1G), and the observed monolayer area expansion accompanied by an ideal mixing reflected in a negative free energy change suggest the fusion of MV although adhesion not progressing into complete fusion cannot be totally ruled out (Fig 1J, L). We then examined the changes in the host membrane fluidity and dipole potential by incorporating a potentiometric dye in membranes, upon the interaction of MVs. We show quantitative evidence that the fusion of bacterial MVs results in enhanced fluidization (depicted in the decrease in fluorescence anisotropy of the dye) and increased dipole potential of the host model membrane (Figure 1H and 1I). The observed range of dipole potential of reconstituted lipid membranes were in line with previous reports [33]. The membrane surface potential of bacterial MVs and lipid membranes was found to be negative (Table S1). Such trans-negative membrane surface potential was reported to be essential for cell-cell fusion [34, 35], also supported by the observed increase in the dipole potential of host model membrane (OLMM) upon the addition of more dipoles from bacterial MVs (Figure 1I). The observed fluidization is supported by the experimentally determined increase in molecular area per lipid as well as elasticity (as seen in reduction in the C_s^{-1} at surface pressure at 35 mN/m) (Figure 1J and 1K). The surface-pressure area isotherm of the lipid fraction of MV devoid of any proteins suggests that the MV membrane is extremely rigid as evident from the low collapse pressure (Figure S2). LPS, the major component

bioRxiv preprint doi: https://doi.org/10.1101/827519; this version posted November 2, 2019. The copyright holder for this preprint (which was not certified by peer review) is the author/funder. All rights reserved. No reuse allowed without permission.

of MV owing to its relatively wider cross-section area and low head-to-tail aspect ratio could be a major contributor towards fluidization as it is known to uniformly adhere and incorporate in egg-PC, DOPG and DOPE containing lipid bilayer [36] all of which are present in the OLMM.

The overall change in the fluidity of the host cell membrane would depend on the degree of interaction between bacterial MVs and the lipids specificity in the OLMM. This could further be influenced by both the lipid head group and the acyl chain length. Indeed, the fusion of bacterial MVs resulted in contrasting effects on fluidity and dipole potential of different lipid membranes. MV fusion to DOPC, Liver PI and DOPG but not BSM membrane, results in enhanced membrane fluidity as well as increased dipole potential arising due to adhesion and incorporation of bacterial MVs (Figure 2, and Figure S3). Slight decrease in area per lipid molecule in case of DOPC and Liver PI membranes suggests adhesion and mixing of lipids from bacterial MVs into monolayer membranes, unlike in case of DOPG membranes, where area expansion was observed suggesting significant interaction with headgroups (Figure3A-3C), reflected in the respective change in elasticity and bending force (Figure 3D-3F, and 3H). The changes in area per lipid molecule are coupled to the degree of interfacial adhesion/fusion of the interacting components [18, 37]. The observed increase in area per lipid molecule is likely due to the formation of inverted cubic structure/aggregates at the adhesion sites resulting in expulsion of some lipids [36, 38], which, also explains the observed relatively higher negative values of ΔG_{Excess}. Likewise, MV fusion to only DPPC membrane results in enhanced fluidization accompanied by increase in interfacial molecular dipoles (Figure 4C). On the contrary, unlike DPPC (a C16 lipid) both shorter and longer acyl chain lengths in DLPC, DMPC and DSPC membrane seem to undergo significant lowering of fluidity as well as largely unchanged to slight increase in dipole potential (Figure 4). Incubation of monolayers with bacterial MVs showed that bacterial MVs have ideal mixing with these lipids at the interfaces as Gibbs free energy mixing was negative in all these membranes (Figure 5I). Maximum change in the bending force and in plane elasticity was observed for DPPC monolayer compared to other lipid monolayers (Figure 5A-5D, and Figure 5J). Together, the data suggest that while MV interaction is facilitated by both zwitterionic and negatively charged head groups, however, an optimum acyl chain length is essential for effective interaction/fusion in line with previous observations [39].

bioRxiv preprint doi: https://doi.org/10.1101/827519; this version posted November 2, 2019. The copyright holder for this preprint (which was not certified by peer review) is the author/funder. All rights reserved. No reuse allowed without permission.

Lipid rafts have also been reported to facilitate the fusion of bacterial MVs [9]. However, this was proved using cholesterol depleting or sequestering agents such as filipin or Methyl-ß-cyclodextrin, which cannot rule out the possibility that disruption of cholesterol on a large scale may affect protein dependent processes not limited to lipid rafts. One way to examine and correlate the exclusive dependence of MV mixing with lipid rafts is by reconstituting minimal systems of lipid raft-like regions without any protein. Bacterial MVs are found to show strongest adhesion to fully disordered membranes devoid of cholesterol (DOPC:BSM:Chol, 5:5:0) accompanied by highest decrease in the fluidity (Figure 6A and 6B). Further, increase in the cholesterol in the membrane lead to decreased adhesion of bacterial MVs to the membrane (Figure 6D and 6G). This is supported by the observed molecular area per lipid expansion observed in surface pressure - area isotherms. The slight expansion in molecular area per lipid seen in fully disordered membrane (DOPC:BSM:Chol, 5:5:0) suggest expulsion of lipids due to steric pressure within monolayer during the adhesion of bacterial MVs at multiple sites (Figure 7A, Figure 6A). Likewise, largest expansion in molecular area per lipid was observed in case of (DOPC:BSM:Chol, 4:4:2) hinting at a strong expulsion of monolayer lipids during the adhesion of bacterial MVs, accompanied by a reduction in the dipole potential of the membrane (Figure 6D, and 6F). This is further supported by positive ΔG_{Excess} and a positive ΔF_b that suggest unfavourable non-ideal mixing (Figure 7B, 7G, and 7H). MV adhesion to membranes containing higher concentration of cholesterol (DOPC:BSM:Chol, 3:3:4) is relatively weaker compared to fully disordered membranes (Figure 6G). The increasing cholesterol levels results in co-existing phase separating regions (L_o and L_d) within the (DOPC:BSM:Chol, 4:4:2 & 3:3:4) membranes, however, the number of the phase separating boundaries is higher in the former. Such differences in the phase separating boundaries would accumulate different degrees of interfacial energy in the membrane, that would facilitate the adhesion of bacterial MVs, which explains the observed variation [40]. Cholesterol amounting to low to moderate levels will not only increase the order in a fluid membrane but also trigger formation of phase separated regions with higher line tension that facilitates the adhesion and fusion of bacterial MVs [40, 41]. On the contrary, higher cholesterol level results in formation of phase separated regions that are larger in size and less in number, reducing the overall interfacial energy and line tension at the phase boundaries that hinder the bacterial MVs fusion to host membrane (Figure 6G). Our results suggest the lipid head-group

bioRxiv preprint doi: https://doi.org/10.1101/827519; this version posted November 2, 2019. The copyright holder for this preprint (which was not certified by peer review) is the author/funder. All rights reserved. No reuse allowed without permission.

preference, elasticity and line tension in membranes showing phase separation could drive the fusion of bacterial MVs to the host membranes.

Increase in the dipole potential of host lipid membrane by fusion of MV is likely to stimulate conformational changes in the membrane bound/inserted receptor proteins [29, 42]. Such conformational changes in transmembrane receptor proteins have been reported to significantly alter the receptor signalling in host cells [43]. Additionally, our study also suggests that MV interaction with lipid rafts/phase boundaries may have an important role in altering host cell signalling [44]. Very recently, *Mycobacterium ulcerans* endotoxin, Mycolactone, was shown to have potent effect on reorganization of raft-like model membranes [45]. Further, bacterial membrane vesicles were found to activate anti-tumour response by inducing production of IFN-γ [46]. It would be interesting to investigate the role of MV induced changes in the dipole potential and elasticity of phagosomal membranes, on the phagosome maturation that involve acidification and fusion with lysosomal vesicles [47]. Although our observations are based on a non-pathogenic strain of *E. coli* as a model bacteria, it is important to note that similar observations can be expected with pathogenic *E. coIi* as they share more than 70% similarity in the protein content of the their membrane vesicles [48, 49]. Further, it is noteworthy that this study focuses on a holistic picture of the consequence of whole MV interaction on host membrane without dissecting the role individual components of MV that may or may not contribute to the observed modulation of host membrane properties. Identifying the potential proteins in the MVs and their contribution to the modulation of the host cell membrane remains an important aspect that would require extensive research.

Significance

Bacterial membrane vesicles (MVs) act as the long-distance delivery tools for virulence factor and thus, directly implicated in host-pathogen interactions and pathogenicity. While the mechanisms of virulence transfer is only recently emerging, however, the interaction of MVs the host cell membrane remains largely unexplored. Whether the bacterial MV interaction can locally modulate the host lipid membrane physicochemical properties (such as fluidity, dipole potential and elasticity) remains unknown. Such alteration in the mechanochemical properties of the host lipid membranes may not only effect signalling but also subsequent process of

bioRxiv preprint doi: https://doi.org/10.1101/827519; this version posted November 2, 2019. The copyright holder for this preprint (which was not certified by peer review) is the author/funder. All rights reserved. No reuse allowed without permission.

phagosome maturation involving fusion of phagosomal membrane with lysosomal membrane compartments. Here, we quantitatively investigate the lipid specificity of *E. Coli* MV interaction and show that MV interaction results in increase in the fluidity, dipole potential and in-plane elasticity (compressibility modulus) of a biologically relevant multi-component host model membrane. The findings could be important for numerous cell signaling processes as well as downstream events involving membrane-membrane fusion such as during the process of phagosome maturation.

bioRxiv preprint doi: https://doi.org/10.1101/827519; this version posted November 2, 2019. The copyright holder for this preprint (which was not certified by peer review) is the author/funder. All rights reserved. No reuse allowed without permission.

Experimental Procedures

Materials

Calcium chloride ($CaCl_2$), HEPES, sodium chloride (NaCl), Lauria Bertini (LB) broth, methanol, chloroform, Nile red were purchased from Himedia, India. Di-8-ANEPPS and DiO were from Thermo Fisher, USA. N-ethylmaleide (NEM), Dimethylsulphoxide (DMSO) and RPM1 media were purchased from Sigma Aldrich, USA. All lipids used in study, 1,2-dioleoyl-*sn*-glycero-3-phosphocholine (DOPC), 1,2-dipalmitoyl-sn-glycero-3-phosphocholine (DPPC), 1,2-dioleoyl-sn-glycero-3-phospho-(1'-rac-glycerol) (DOPG), L-α-phosphatidylinositol (Liver, Bovine) (Liver PI), Sphingomyelin from Brain, Porcine (BSM), cholesterol, 1,2-dioleoyl-sn-glycero-3-phosphoethanolamine (DOPE) were purchased from Avanti Polar lipids, USA. Monocytic leukemia cell lines (THP-1) were purchased from the National Center of Cell Science, Pune, India.

Preparation of Buffers and Solutions

Membrane vesicle (MV) buffer was prepared by dissolving 10 mM of HEPES, 2 mM of $CaCl_2$ and 150 mM of NaCl in autoclaved distilled water and adjusting the pH at 7.4. NEM solution was made by dissolving NEM in miliQ water to make 3mM concentration of stock solution. For each experiment, NEM solution should be freshly prepared. Nile dissolved in DMSO (dimethylsulphoxide) to the final concentration of 100 nM. DiO labelling solution was prepared by dissolving 1mg DiO in 1 mL of DMSO.

Membrane Vesicles Purification from Bacteria

For membrane vesicle formation, Gram negative bacteria, *E. coli* were used. The methodology for MV vesiculation and isolation was adopted from the procedure described by Sezgin et. al. [50] with some modification and optimization that allowed us to obtain reasonably homogenous pool of MV size in the range of 200-250 nm. We optimized the method that allowed us to isolate bacterial MVs without the usage of ultracentrifugation. Bacterial cells were cultured in Luria Bertani (LB) broth by inoculating a single colony of *E. coli* from slant culture, shaking at 120 rpm and incubated at 37°C. Cells were grown until optical density of culture reached to a value of 1.0 where, *E. coli* are in mid-exponential phase of growth. Cells were collected from

bioRxiv preprint doi: https://doi.org/10.1101/827519; this version posted November 2, 2019. The copyright holder for this preprint (which was not certified by peer review) is the author/funder. All rights reserved. No reuse allowed without permission.

media by mild centrifugation at 5000 rpm for 10 minutes then supernatant were thrown. The pellet was again re-suspended in 50 mL membrane vesicles (MV) buffer (pH-7.4). Cells were again centrifuged and washed twice in MV buffer at 5000 rpm for 10 minutes, then media free cells were present in pallet. Pellet of bacterial cells were then treated with 30 ml of 3mM of N-ethyl-malemide (NEM) solution. N-ethyl maleimide (NEM) is well optimized chemical vesiculant for obtaining Giant Plasma Membrane Vesicles (GPMV) from eukaryotic cell membranes. The choice of NEM as a chemical vesiculant is justified by the fact that it is known not to cross-link with proteins and aldehydes or cause coupling of phosphatidylethanolamine to proteins or depalmitoylation. Cells were then incubated in NEM containing MV buffer for 1 hour for vesiculation of bacterial MVs from bacterial cells. Vesiculated bacterial MVs in cells were isolated by high-speed centrifugation at 18000g for 2 hours at 4˚C and supernatant containing membrane vesicles (bacterial MVs) was collected. The bacterial MVs in supernatant was concentrated by using a 10 kD cut-off filter through 0.22 µM filter paper for the uniformity in size of bacterial MVs.

For isotherm analysis, we sought to isolate lipid molecules from bacterial MVs by following Folch method solvent system [51, 52] . 300 µL of freshly prepared MV solution in MV buffer was dried with nitrogen gas stream and kept in vacuum chamber overnight for water elimination. For vesicle opening, 300 µL chloroform was then added to the dried bacterial MVs and bath sonicated for 30 minutes at constant pulse. Post sonication, the solution was transferred to another vial and again dried with nitrogen gas. Chloroform (320 µL) and ice-cold methanol (160 µL) were subsequently added in 2:1 v/v ratio to dried sample and incubated for 20 minutes on ice with occasional vortex mixing followed by addition of 150 µL deionized water and kept on ice for additional 10 minutes with occasional agitation. The mixture was then centrifuged at 1500 rpm for 5 minutes for removal of the upper polar phase containing salts and proteins. For additional washing, 2:1 v/v chloroform and ice cold methanol was again added and the above process was repeated. After removal of the upper phase, the final lower organic phase containing lipids was dried with nitrogen stream and suspended in 100 µL chloroform. It was kept at -20ºC for future use. Extracted lipid estimation of bacterial MVs is shown in the supporting information.

Size Distribution, Detection and Fluorescence Microscopy of MV

bioRxiv preprint doi: https://doi.org/10.1101/827519; this version posted November 2, 2019. The copyright holder for this preprint (which was not certified by peer review) is the author/funder. All rights reserved. No reuse allowed without permission.

The detection and size of purified bacterial MVs in supernatant buffer was confirmed by fluorescence microscopy and dynamic light scattering (DLS) experiments. Fluorescence imaging and fluorimetry were done by incorporating a membrane binding dye Nile red to bacterial MVs. In sample preparation for imaging and fluorimetry, 990 µL of bacterial MVs in MV buffer were incubated with 10 µL of Nile red (100 µM) in 100/1 (v/v) ratio of MV/dye for 30 minutes. For control sample to perform fluorimetry for Nile red in MV was done by taking 10 µL dye in 990 µL of MV buffer. For fluorescence imaging 10 µL of labelled bacterial MVs were dropped on coverslip to visualize MV under fluorescence microscope (Olympus, IX71) with oil immersed 63x magnification of objective. Fluorescence intensity measurements of bacterial MVs were carried out by checking fluorescence intensity of Nile red incorporated bacterial MVs in MV buffer with respect to control sample i.e. MV buffer with Nile red. Excitation and emission spectra were optimized at 530 nm and 570 nm respectively.

For size distribution of bacterial MVs, 1 mL of MV in MV buffer were filled in quartz cuvette and allowed to equilibrated for 5 minutes. DLS was measured by Zetasizer Nano ZS (Malvern Zetasizer Nano ZS90, Netherland) with 633 nm Laser by electrophoretic mobility of bacterial MVs in solution.

Electron Microscopy of Bacterial MVs

To visualize the morphology of bacterial MVs, we performed scanning electron microscopy. For sample preparation, 10 µL of purified and filtered MV suspension was spread on a small glass slide then the sample on glass slide was fixed with 2.5% of glutaraldehyde solution and incubated at 4°C for 12 hours. After fixation, sample was washed with 1% tannic acid solution then again washed with distilled water. Finally, sample was dehydrated sequentially by dipping them in order of 30%, 50%, 70%, 90% and absolute alcohol solutions. Before, electron microscopy bacterial MVs on glass slide were coated by sputtering with gold coating and visualized under FE- SEM (Nova NanoSEM 450/FE).

Fluorescence Labeling of Bacterial MVs

Purified bacterial MVs were labelled with a lipophilic dye DiO to study binding of bacterial MVs with reconstituted membranes. DiO dye mixed to MV in ratio of 1:100 v/v dropwise with constant stirring at 37°C for 30 minutes for incorporation of dye in

bioRxiv preprint doi: https://doi.org/10.1101/827519; this version posted November 2, 2019. The copyright holder for this preprint (which was not certified by peer review) is the author/funder. All rights reserved. No reuse allowed without permission.

bacterial MVs. To separate unlabeled dye from labelled bacterial MVs, the mixture was washed with PBS buffer four times using 10kD cut-off concentrators (Merck-millipore). Labelled bacterial MVs were kept at 4°C and can be stored upto one week for further experiments.

Fusion of Bacterial MVs to Macrophage Cells

To check the fusion of bacterial MVs with macrophages cells, fluorescence intensity was measured. Differentiated macrophages (THP-1) were freshly cultured in RPM1 media from the maintained culture. Cells were grown up to 70% of confluence. Cells were then washed with 2 mL PBS (pH – 7.4) then again washed with 2 mL of MV buffer. In last step cells were washed with the 2 mL of MV buffer containing bacterial MVs for fusion study of MV in cells. For Sample preparation for fluorimetry from MV treated cells, 100 µL of cell soup was taken, re-suspended in 900 µL of MV buffer and 10 µL of Nile red. For control only 100 µL of MV, 900 µL of MV buffer and 10 µL of Nile red was mixed. Fluorescence intensity was then measured at 530 nm of excitation spectrum and 570 emission spectra in fluorimetry at time t=0. Then the same above preparation were done in every 30 minutes of interval and intensity was observed for fusion study.

Reconstitution of Fluorescence Labelled Giant Unilamellar Vesicles (GUVs)

Giant unilamellar vesicles (GUVs) were prepared using polyvinyl alcohol (PVA) gel-assisted method as previously described by Weinberger *et. al.* with slight modifications[53]. PVA-coating on the surface of glass slides were used as film for swelling of lipid film for reconstitution of GUVs. To prepare PVA coated slides, PVA was dissolved in deionized water in 5% w/w ratio of PVA/water with constant stirring at 90°C. From this PVA solution, 200-300 µL is evenly spread on the glass slide and dried in oven at 50°C for 30 minutes which makes a thin film over the surface of slide. This dried PVA-coated slides then cleaned with UV for 15 minutes to prevent dewetting of PVA coating. Now, 20 µL of Lipid solution in chloroform (1mg/mL) doped with 1 mole % Rhodamine-PE of total lipid mole fraction was smeared on PVA-coated slide with Hamilton syringe. Residual chloroform on the PVA-coated slide was evaporated by keeping the slide in vacuum chamber for 2 to 3 hours. A chamber on the lipid spread PVA-coated slide was made using nitrile ring sealed by using a second coverslip and

bioRxiv preprint doi: https://doi.org/10.1101/827519; this version posted November 2, 2019. The copyright holder for this preprint (which was not certified by peer review) is the author/funder. All rights reserved. No reuse allowed without permission.

clips as sealant. This lipid film was then swelled by filling the chamber with 1 mL of 10 mM phosphate buffer saline (PBS) at pH of 7.4 for vesiculation. After 30 minutes the chamber was gently agitated and the buffer of chamber was collected in microcentrifuge tubes containing GUVs.

Confocal Fluorescence Microscopy

Custom made open chambers were used for incubating the GUVs and DiO -MVs. The cover slip was rinsed with 70% ethanol and air-dried. 10 µL of the GUVs from the was added to 90 µL of equi-osmolar MV buffer containing bacterial MVs, and were incubated for 15-20 mins and allowed to equilibrate. Imaging was performed using a Leica TCS-SP8 confocal instrument using appropriate lasers for rhodamine-PE (DPSS-561) and DiO (argon-488). An identical laser power and gain settings were used during the course of all the experiments. The image processing was done using ImageJ.

Preparation of Large Unilamellar Vesicles (LUVs)

Each specific type of LUVs was prepared with the help of different phospholipids in total number of 120 nmoles by corresponding lipids dissolved in chloroform. The mixture of lipids were doped with 1 mole% of di-8-ANEPPS and for background correction only lipids were mixed free of dye. The prepared mixtures then dried with steady nitrogen gas stream and kept in vacuum for 3 hours for complete evaporation of residual solvent from the lipid mixtures. Thereafter, lipids were re-suspended in 500 uL of MV buffer (pH-7.4) for hydration of lipids then suspension was heated in water bath for 15 minutes at 45 ºC. After heating, samples were vortexed for 5 minutes and sonicated for 2 minutes at 0.9 sec pulse rate and 100% amplitude to produce LUVs of roughly 500 nm diameter which was confirmed by dynamic light scattering (DLS).

Anisotropy and Dipole Potential Measurement of Reconstituted Membranes

Anisotropy and dipole potential measurements of specific lipid membranes were done by fluorescence spectroscopy. For these studied, reconstituted LUVs with specific composition of phospholipids were used and incubated with bacterial MVs. For each sample preparation, 200 µM of LUVs without bacterial MVs was taken as control whereas the same sample treated with 0.2 mg/mL and 0.6 mg/mL of bacterial MVs were the test samples. Now, these samples were incubated for 1 hour at 25°C in dark before

bioRxiv preprint doi: https://doi.org/10.1101/827519; this version posted November 2, 2019. The copyright holder for this preprint (which was not certified by peer review) is the author/funder. All rights reserved. No reuse allowed without permission.

fluorimetric quantification i.e. anisotropy and dipole potential measurements. All measurements were done in 500 µL of quartz cuvette by using LS55 PerkinElmer spectrophotometer. For dipole potential study, excitation spectra were obtained by scanning the sample with 5 nm slit bandpass at 240 nm/s scan speed and the emission wavelength was fixed at 670 nm to avoid membrane fluidity effects. Background was corrected by subtracting the intensities of test samples containing di-8-ANEPPS with sample without the dye. Dipole potential was calculated by taking ratio (R), of emission intensities at 670 nm excited at 420 nm and 520 nm respectively for each sample. All values of anisotropy were calculated automatically by the instrument by using the following equation[17]:

$$r = \frac{I_{VV} - GI_{VH}}{I_{VV} + 2GI_{VH}}$$

Where, I_{VH} and I_{VV} are the measured fluorescence intensities with excitation polarizer oriented vertically and emission polarizer oriented horizontally and vertically, respectively. G (= I_{HV}/I_{HH}) is the grating correction factor and is the ratio of the efficiencies of the detection system for vertically and horizontally polarized light. All experiments were conducted with multiple independent sets for each lipid.

Langmuir Blodgett Monolayer Preparation and Isotherm Analysis

Langmuir monolayer films were prepared using a microprocessor controlled Teflon molded LB trough (Apex Instruments, India) having inner working dimension of 305 mm X 105 mm. The rectangular trough was equipped with two movable Teflon bars which provided symmetrical compression speed and the surface pressure being measured with an accuracy of ±0.05 mN/m by a Wilhelmy plate (filter paper of dimensions 10 x 25 mm^2) connected to a highly sensitive electronic balance system. The entire system was set inside a transparent glove box. The trough was cleaned subsequently with methanol, ethanol and ultrapure water to make it dust free and utmost care was taken to avoid internal and external vibration during the experiments. MV buffer was used as the subphase whose temperature was maintained at 25 ºC. Prior to each isotherm run, the interface cleaning operation was performed by compressing the two bars to a maximum and checking the surface pressure. Lipid solution at 1 mg/ml concentration was spread drop by drop on the air/ buffer interface until a surface pressure of 2-3 mN/m was

bioRxiv preprint doi: https://doi.org/10.1101/827519; this version posted November 2, 2019. The copyright holder for this preprint (which was not certified by peer review) is the author/funder. All rights reserved. No reuse allowed without permission.

reached and waited for 15-20 minutes for the chloroform to evaporate off and π to come down to 0 mN/m. 10 µL MV solution (2 µM) was injected into the subphase prior to monolayer compression. The subphase was constantly agitated using a magnetic bead stirrer at the bottom of the trough for uniform distribution of bacterial MVs. π-A Isotherm run was started by compressing the monolayer at a constant speed of 8 mm/min. Isotherms were recorded until collapse pressure π_c was reached. Thorough cleaning of the trough was followed after each run. Each isotherm was repeated independently to ensure consistency. Isotherm data were used to calculate compressibility modulus (C_s^{-1}), excess Gibb's free energy of mixing (ΔG_{Excess}) and bending force (ΔF_b).

Statistical Analysis

Data were analyzed by one-way analysis of variance (ANOVA) using Origin 8.5 software. P-values <.0.5 were considered were considered statistically significant. All values were reported as mean ± SE from appropriate sample size and three independent experiments as indicated and where (***) depicts $p<0.001$, (**) $p<0.01$ and (*) $p<0.05$.

Acknowledgements

We would like to thank Dr Hirak Chakraborty, Dr Yusuf Akhter and Dr Bhavani Shankar Sahu for critical reading and stimulating discussion on the manuscript. We would like to gratefully acknowledge the financial support received from the Department of Science and Technology and Department of Biotechnology, Govt. of India. AP, AT and TM acknowledge MHRD for the GATE fellowship.

Author Contributions

AP and MS conceived the idea and designed the research. AP, AT and KS prepared carried out the characterization of bacterial MVs. DKS helped with MV characterization. AP and NK performed fluorimetry experiments. AP and AT performed labelling of bacterial MVs and imaging experiments. AP and TM performed monolayer experiments. AP, AT, TM and MS analysed the data. AP, AT, TM and MS wrote the manuscript.

bioRxiv preprint doi: https://doi.org/10.1101/827519; this version posted November 2, 2019. The copyright holder for this preprint (which was not certified by peer review) is the author/funder. All rights reserved. No reuse allowed without permission.

Declaration of Interests

Authors declare no competing interests.

References

1.1. T. J. Beveridge, *Journal of bacteriology*, 1999, **181**, 4725-4733.
2. C. Schwechheimer and M. J. Kuehn, *Nature Reviews Microbiology*, 2015, **13**, 605.
3. A. Kulp and M. J. Kuehn, *Annual review of microbiology*, 2010, **64**, 163-184.
4. M. Toyofuku, N. Nomura and L. Eberl, *Nature Reviews Microbiology*, 2018, 1.
5. K. Koeppen, T. H. Hampton, M. Jarek, M. Scharfe, S. A. Gerber, D. W. Mielcarz, E. G. Demers, E. L. Dolben, J. H. Hammond and D. A. Hogan, *PLoS pathogens*, 2016, **12**, e1005672.
6. I. A. MacDonald and M. J. Kuehn, *Research in microbiology*, 2012, **163**, 607-618.
7. M. K. Chattopadhyay and M. V. Jagannadham, *Frontiers in microbiology*, 2015, **6**, 758.
8. M. Kaparakis-Liaskos and R. L. Ferrero, *Nature reviews Immunology*, 2015, **15**, 375.
9. J. M. Bomberger, D. P. MacEachran, B. A. Coutermarsh, S. Ye, G. A. O'Toole and B. A. Stanton, *PLoS pathogens*, 2009, **5**, e1000382.
10. J. Jäger, S. Keese, M. Roessle, M. Steinert and A. B. Schromm, *Cellular microbiology*, 2015, **17**, 607-620.
11. E. J. O'donoghue and A. M. Krachler, *Cellular microbiology*, 2016, **18**, 1508-1517.
12. P. Greenspan, E. P. Mayer and S. D. Fowler, *The Journal of cell biology*, 1985, **100**, 965-973.
13. G. Van Meer, D. R. Voelker and G. W. Feigenson, *Nature reviews Molecular cell biology*, 2008, **9**, 112.
14. E. J. O'Donoghue, N. Sirisaengtaksin, D. F. Browning, E. Bielska, M. Hadis, F. Fernandez-Trillo, L. Alderwick, S. Jabbari and A. M. Krachler, *PLoS pathogens*, 2017, **13**, e1006760.
15. S. Bandari, H. Chakraborty, D. F. Covey and A. Chattopadhyay, *Chemistry and physics of lipids*, 2014, **184**, 25-29.
16. E. Gross, R. S. Bedlack Jr and L. M. Loew, *Biophysical journal*, 1994, **67**, 208-216.
17. T. Starke-Peterkovic, N. Turner, M. F. Vitha, M. P. Waller, D. E. Hibbs and R. J. Clarke, *Biophysical journal*, 2006, **90**, 4060-4070.
18. H. Brockman, *Current opinion in structural biology*, 1999, **9**, 438-443.
19. D. Allende, A. Vidal and T. J. McIntosh, *Trends in biochemical sciences*, 2004, **29**, 325-330.
20. R. E. Brown and H. L. Brockman, in *Lipid Rafts*, Springer, 2007, pp. 41-58.
21. J. M. Smaby, V. S. Kulkarni, M. Momsen and R. E. Brown, *Biophysical journal*, 1996, **70**, 868-877.
22. S.-s. Feng, *Langmuir*, 1999, **15**, 998-1010.
23. F. Goodrich, *Vol. I*, 1957, 85.
24. C. Peetla, S. Jin, J. Weimer, A. Elegbede and V. Labhasetwar, *Langmuir*, 2014, **30**, 7522-7532.
25. B. A. Lewis and D. M. Engelman, *Journal of molecular biology*, 1983, **166**, 211-217.
26. T. Miyoshi and S. Kato, *Langmuir*, 2015, **31**, 9086-9096.
27. L. Zhao and S.-S. Feng, *Journal of colloid and interface science*, 2004, **274**, 55-68.
28. K. Simons and E. Ikonen, *nature*, 1997, **387**, 569.
29. Y. A. Ermakov, A. Z. Averbakh, A. I. Yusipovich and S. Sukharev, *Biophysical journal*, 2001, **80**, 1851-1862.
30. D. Chen and M. M. Santore, *Proceedings of the National Academy of Sciences*, 2014, **111**, 179-184.
31. J. Ge and F. Shao, *Cellular microbiology*, 2011, **13**, 1870-1880.
32. A. Hubber and C. R. Roy, *Annual review of cell and developmental biology*, 2010, **26**, 261-283.

bioRxiv preprint doi: https://doi.org/10.1101/827519; this version posted November 2, 2019. The copyright holder for this preprint (which was not certified by peer review) is the author/funder. All rights reserved. No reuse allowed without permission.

33. L. Wang, P. S. Bose and F. J. Sigworth, *Proceedings of the National Academy of Sciences*, 2006, **103**, 18528-18533.
34. T. Asawakarn, J. Cladera and P. O'Shea, *Journal of Biological Chemistry*, 2001, **276**, 38457-38463.
35. A. V. Samsonov, P. K. Chatterjee, V. I. Razinkov, C. H. Eng, M. Kielian and F. S. Cohen, *Journal of virology*, 2002, **76**, 12691-12702.
36. K. Nomura, T. Inaba, K. Morigaki, K. Brandenburg, U. Seydel and S. Kusumoto, *Biophysical journal*, 2008, **95**, 1226-1238.
37. M. Mura, S. R. Dennison, A. V. Zvelindovsky and D. A. Phoenix, *Biochimica et Biophysica Acta (BBA)-Biomembranes*, 2013, **1828**, 586-594.
38. P. G. Adams, L. Lamoureux, K. L. Swingle, H. Mukundan and G. A. Montaño, *Biophysical journal*, 2014, **106**, 2395-2407.
39. J. A. Szule, N. L. Fuller and R. P. Rand, *Biophysical journal*, 2002, **83**, 977-984.
40. S.-T. Yang, V. Kiessling and L. K. Tamm, *Nature communications*, 2016, **7**, 11401.
41. H. J. Risselada, G. Marelli, M. Fuhrmans, Y. G. Smirnova, H. Grubmüller, S. J. Marrink and M. Müller, *PLoS One*, 2012, **7**, e38302.
42. S. I. Sukharev, W. J. Sigurdson, C. Kung and F. Sachs, *The Journal of general physiology*, 1999, **113**, 525-540.
43. Y. Zhou, C.-O. Wong, K.-j. Cho, D. Van Der Hoeven, H. Liang, D. P. Thakur, J. Luo, M. Babic, K. E. Zinsmaier and M. X. Zhu, *Science*, 2015, **349**, 873-876.
44. T. Kovács, G. Batta, T. Hajdu, Á. Szabó, T. Váradi, F. Zákány, I. Csomós, J. Szöllősi and P. Nagy, *Scientific reports*, 2016, **6**, 35850.
45. M. Nitenberg, A. Benarouche, O. Maniti, E. Marion, L. Marsollier, J. Géan, E. J. Dufourc, J.-F. Cavalier, S. Canaan and A. P. Girard-Egrot, *PLoS pathogens*, 2018, **14**, e1006814.
46. O. Y. Kim, H. T. Park, N. T. H. Dinh, S. J. Choi, J. Lee, J. H. Kim, S.-W. Lee and Y. S. Gho, *Nature communications*, 2017, **8**, 626.
47. B. E. Steinberg, N. Touret, M. Vargas-Caballero and S. Grinstein, *Proceedings of the National Academy of Sciences*, 2007, **104**, 9523-9528.
48. E. Y. Lee, J. Y. Bang, G. W. Park, D. S. Choi, J. S. Kang, H. J. Kim, K. S. Park, J. O. Lee, Y. K. Kim and K. H. Kwon, *Proteomics*, 2007, **7**, 3143-3153.
49. F. B. Scorza, F. Doro, M. J. Rodríguez-Ortega, M. Stella, S. Liberatori, A. R. Taddei, L. Serino, D. G. Moriel, B. Nesta and M. R. Fontana, *Molecular & Cellular Proteomics*, 2007.
50. E. Sezgin, H.-J. Kaiser, T. Baumgart, P. Schwille, K. Simons and I. Levental, *nature protocols*, 2012, **7**, 1042.
51. J. Folch, M. Lees and G. Sloane Stanley, *J biol Chem*, 1957, **226**, 497-509.
52. A. Reis, A. Rudnitskaya, G. J. Blackburn, N. M. Fauzi, A. R. Pitt and C. M. Spickett, *Journal of lipid research*, 2013, **54**, 1812-1824.
53. A. Weinberger, F.-C. Tsai, G. H. Koenderink, T. F. Schmidt, R. Itri, W. Meier, T. Schmatko, A. Schröder and C. Marques, *Biophysical journal*, 2013, **105**, 154-164.

bioRxiv preprint doi: https://doi.org/10.1101/827519; this version posted November 2, 2019. The copyright holder for this preprint (which was not certified by peer review) is the author/funder. All rights reserved. No reuse allowed without permission.

Figures

Figure 1

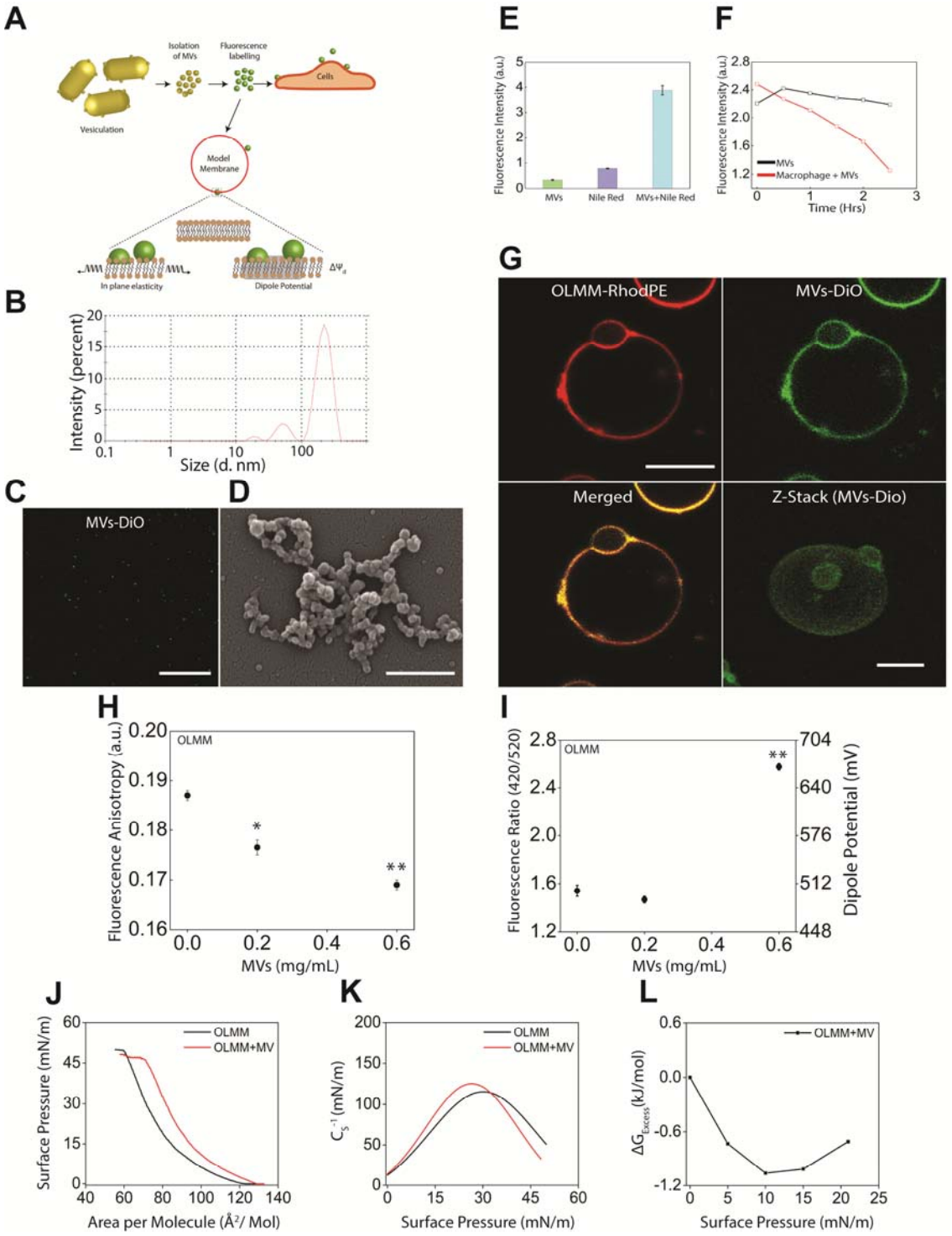

bioRxiv preprint doi: https://doi.org/10.1101/827519; this version posted November 2, 2019. The copyright holder for this preprint (which was not certified by peer review) is the author/funder. All rights reserved. No reuse allowed without permission.

Figure 2

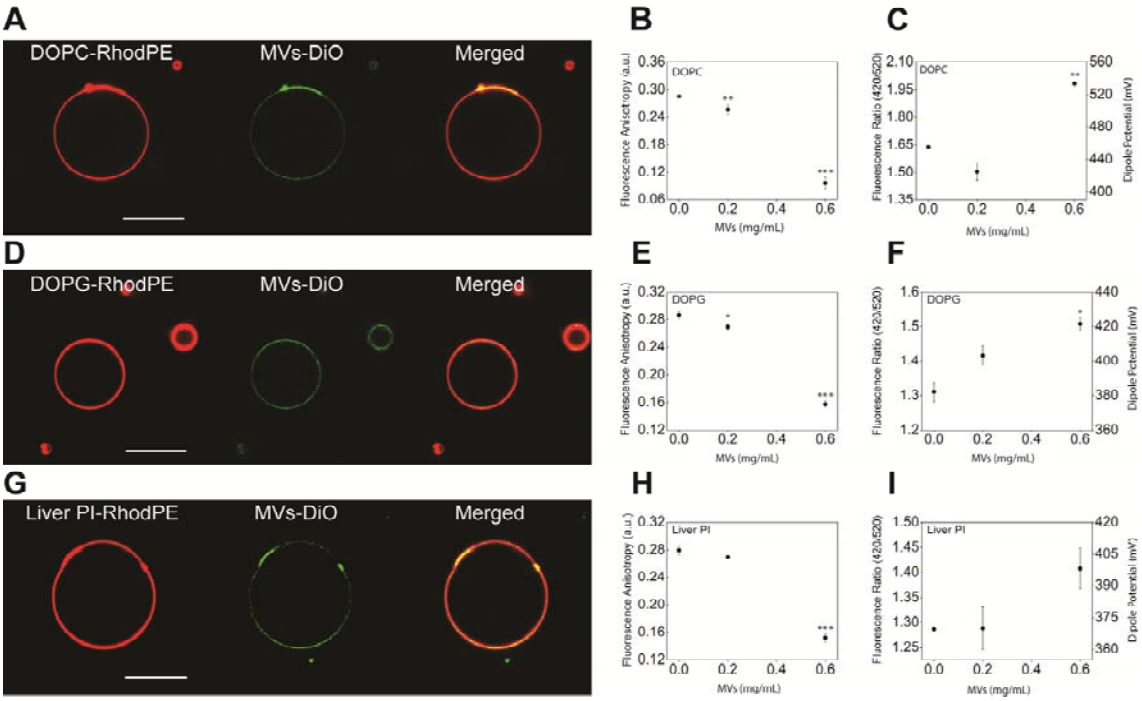

bioRxiv preprint doi: https://doi.org/10.1101/827519; this version posted November 2, 2019. The copyright holder for this preprint (which was not certified by peer review) is the author/funder. All rights reserved. No reuse allowed without permission.

Figure 3.

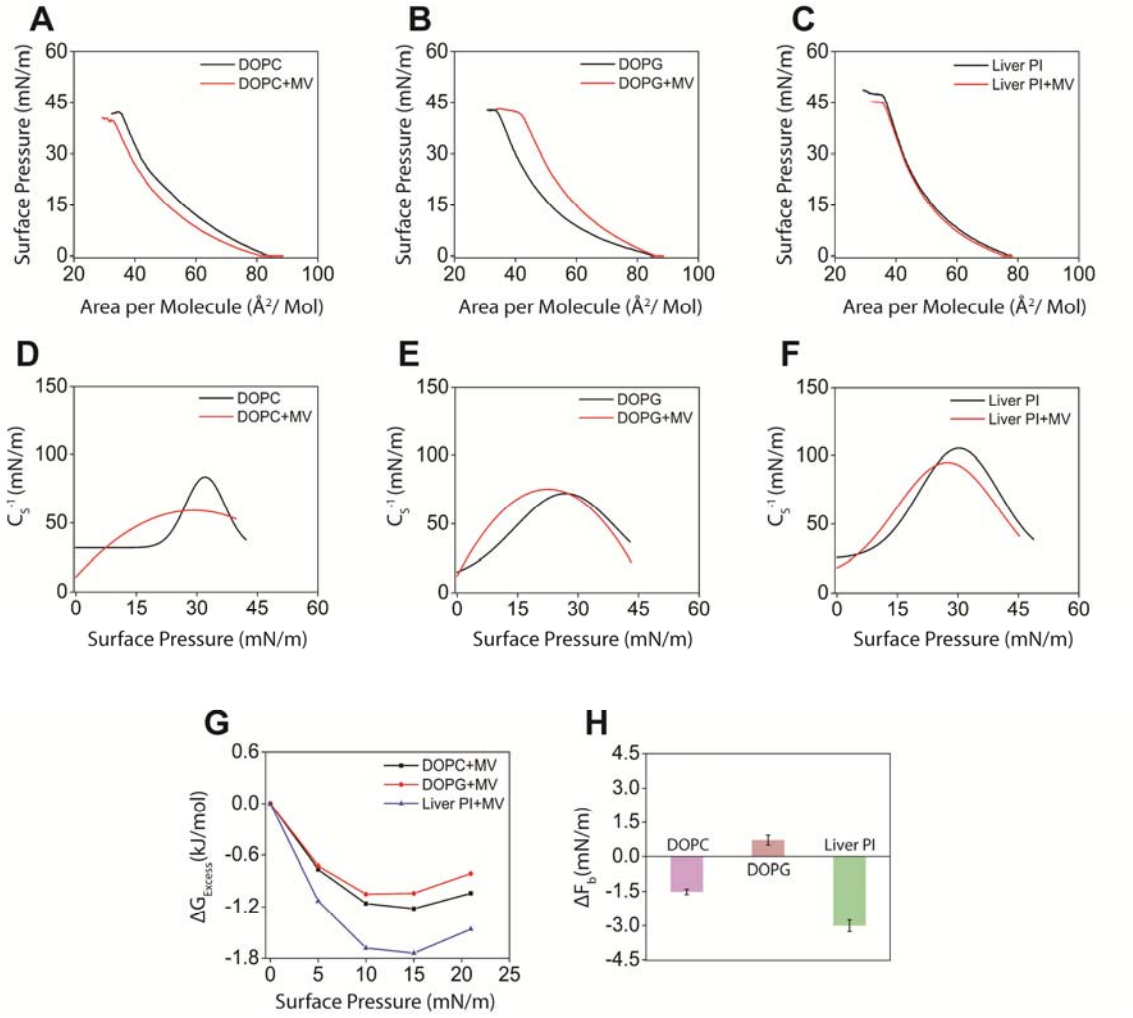

bioRxiv preprint doi: https://doi.org/10.1101/827519; this version posted November 2, 2019. The copyright holder for this preprint (which was not certified by peer review) is the author/funder. All rights reserved. No reuse allowed without permission.

Figure 4

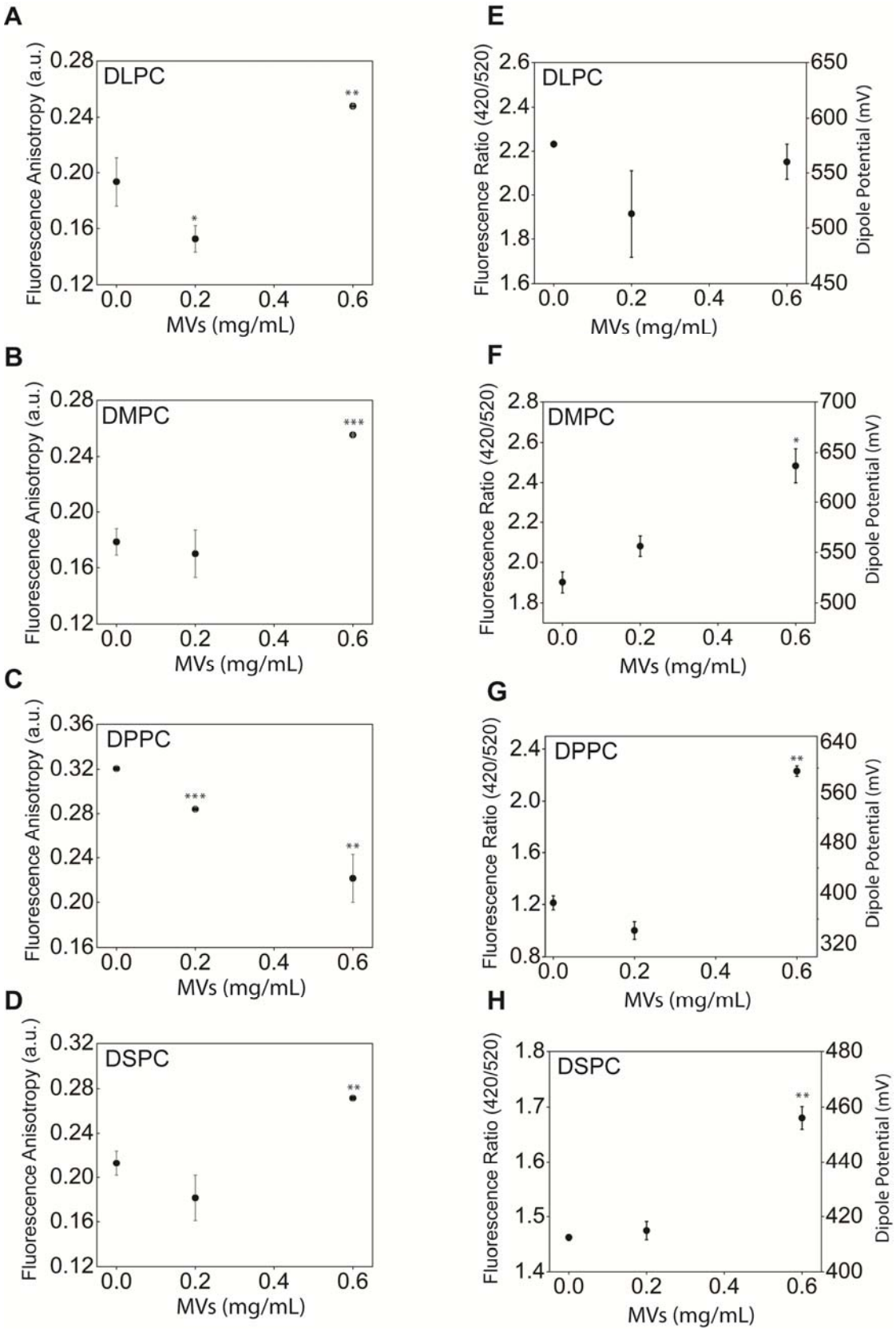

bioRxiv preprint doi: https://doi.org/10.1101/827519; this version posted November 2, 2019. The copyright holder for this preprint (which was not certified by peer review) is the author/funder. All rights reserved. No reuse allowed without permission.

bioRxiv preprint doi: https://doi.org/10.1101/827519; this version posted November 2, 2019. The copyright holder for this preprint (which was not certified by peer review) is the author/funder. All rights reserved. No reuse allowed without permission.

Figure 5

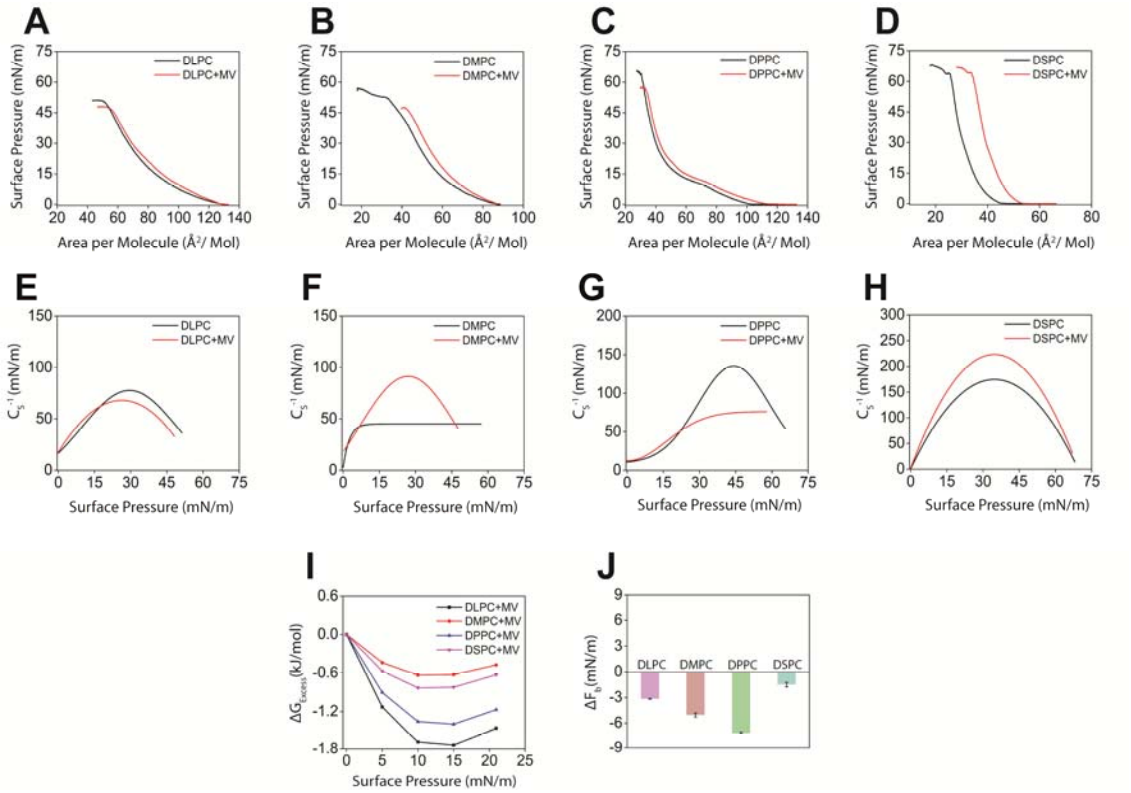

bioRxiv preprint doi: https://doi.org/10.1101/827519; this version posted November 2, 2019. The copyright holder for this preprint (which was not certified by peer review) is the author/funder. All rights reserved. No reuse allowed without permission.

Figure 6

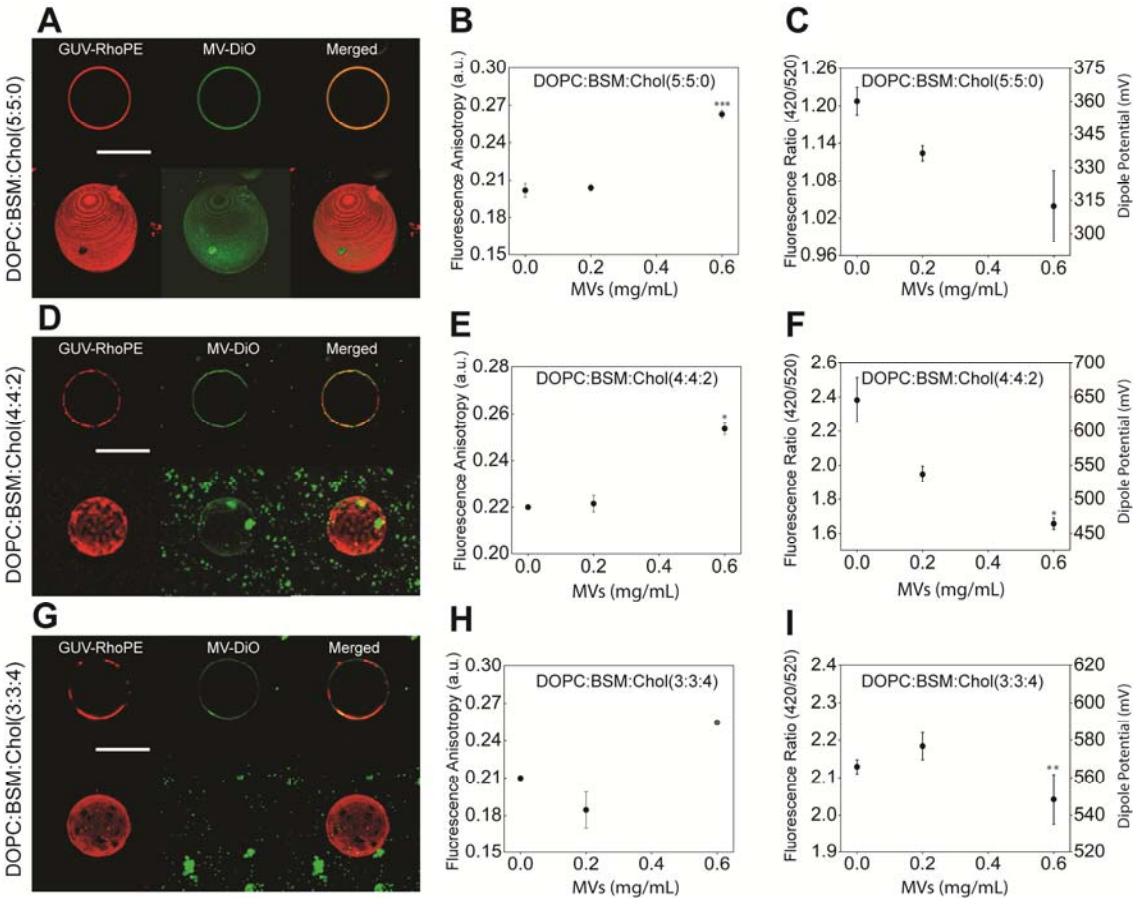

bioRxiv preprint doi: https://doi.org/10.1101/827519; this version posted November 2, 2019. The copyright holder for this preprint (which was not certified by peer review) is the author/funder. All rights reserved. No reuse allowed without permission.

Figure 7